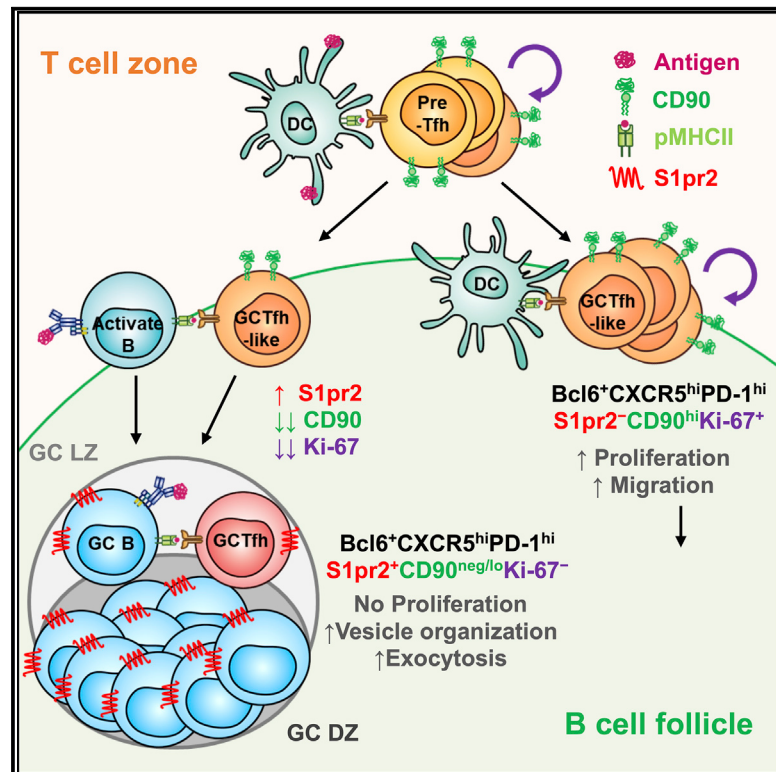


Primary germinal center-resident T follicular helper cells are a physiologically distinct subset of CXCR5^{hi}PD-1^{hi} T follicular helper cells

Graphical abstract



Authors

Chen-Hao Yeh, Joel Finney,
Takaharu Okada, Tomohiro Kuroasaki,
Garnett Kelsoe

Correspondence

ghkelsoe@duke.edu

In brief

T follicular helper (Tfh) cells within the germinal center (GC) arbitrate antibody affinity maturation. Yeh et al. utilize various models to distinguish GC-resident Tfh cells, showing that the previous phenotypic definition of GCTfh cells includes a large subset that does not enter GCs. These CD90^{hi} Tfh cells have different developmental requirements and activities than the rarer GC-resident Tfh cells (CD90^{neg/lo}), implying distinct functions.

Highlights

- Primary Bcl6⁺CXCR5^{hi}PD-1^{hi} Tfh cells encompass both GC-resident and nonresident cells
- GC-resident Tfh cells are S1pr2⁺CD90^{neg/lo}; nonresident, GCTfh-like are S1pr2⁻CD90^{hi}
- CD90^{neg/lo} GCTfh and CD90^{hi} GCTfh-like cells have distinct developmental requirements
- GCTfh and GCTfh-like cells have distinct TCR repertoires and transcriptomic profiles



Article

Primary germinal center-resident T follicular helper cells are a physiologically distinct subset of CXCR5^{hi}PD-1^{hi} T follicular helper cells

Chen-Hao Yeh,¹ Joel Finney,¹ Takaharu Okada,^{2,3} Tomohiro Kurosaki,^{4,5} and Garnett Kelsoe^{1,6,7,*}

¹Department of Immunology, Duke University School of Medicine, Durham, NC 27710, USA

²Laboratory for Tissue Dynamics, RIKEN Center for Integrative Medical Sciences (IMS), Yokohama, Kanagawa 230-0045, Japan

³Graduate School of Medical Life Science, Yokohama City University, Yokohama, Kanagawa 230-0045, Japan

⁴Laboratory of Lymphocyte Differentiation, WPI Immunology Frontier Research Center, Osaka University, Osaka 565-0871, Japan

⁵Laboratory for Lymphocyte Differentiation, RIKEN Center for Integrative Medical Sciences (IMS), Yokohama, Kanagawa 230-0045, Japan

⁶Department of Surgery and Duke University Human Vaccine Institute, Duke University School of Medicine, Durham, NC 27710, USA

⁷Lead contact

*Correspondence: ghkelsoe@duke.edu

<https://doi.org/10.1016/j.immuni.2021.12.015>

SUMMARY

T follicular helper (Tfh) cells are defined by a Bcl6⁺CXCR5^{hi}PD-1^{hi} phenotype, but only a minor fraction of these reside in germinal centers (GCs). Here, we examined whether GC-resident and -nonresident Tfh cells share a common physiology and function. Fluorescently labeled, GC-resident Tfh cells in different mouse models were distinguished by low expression of CD90. CD90^{neg/lo} GCTfh cells required antigen-specific, MHCII⁺ B cells to develop and stopped proliferating soon after differentiation. In contrast, nonresident, CD90^{hi} Tfh (GCTfh-like) cells developed normally in the absence of MHCII⁺ B cells and proliferated continuously during primary responses. The TCR repertoires of both Tfh subsets overlapped initially but later diverged in association with dendritic cell-dependent proliferation of CD90^{hi} GCTfh-like cells, suggestive of TCR-dependency seen also in TCR-transgenic adoptive transfer experiments. Furthermore, the transcriptomes of CD90^{neg/lo} and CD90^{hi} GCTfh-like cells were enriched in different functional pathways. Thus, GC-resident and nonresident Tfh cells have distinct developmental requirements and activities, implying distinct functions.

INTRODUCTION

T follicular helper cells represent a differentiation lineage distinct from other CD4⁺ helper T cell types, with Bcl6 serving as the lineage-defining transcription factor (Johnston et al., 2009; Nurieva et al., 2009; Yu et al., 2009). The Tfh fate decision appears to be made prior to Bcl6 expression and may be determined by the initial strength of T-cell antigen receptor (TCR) signaling when encountering antigen-presenting dendritic cells (DCs) (Choi et al., 2013; Tubo et al., 2013). Whereas non-Tfh effector cells (e.g., Th1, Th2, and Th17) predominantly emigrate to distal sites, Tfh cells largely remain *in situ* and play a crucial role in T-dependent B cell responses (Crotty, 2014). Early Tfh cells express the chemokine receptor CXCR5, enabling them to migrate to the B cell follicle border. There, they interact with activated B cells, undergo further maturation, and subsequently penetrate the follicle, where a subset of Tfh cells help initiate germinal centers (GCs) (Ansel et al., 1999; Breitfeld et al., 2000; Haynes et al., 2007; Scherli et al., 2000). In organized GCs, Tfh cells residing within the GC light zone (LZ) are necessary for the maintenance of the GC reaction. These GCTfh cells are thought to arbitrate

affinity-driven competition among GC B cells and to influence GCB cell differentiation into plasma cells or memory B cells in a manner that reflects the quality of cognate interaction between GCTfh and GCB cells (Crotty, 2014; Wan et al., 2019). Whereas all Tfh cells share a defining Bcl6⁺CXCR5⁺ signature, not every Tfh cell enters or remains in GCs (Crotty, 2019; Shulman et al., 2013). Tfh cells that do not enter GCs are unlikely to provide direct selection signals to GCB cells; instead, these Tfh may have effector activities outside GCs and may be a source of memory Tfh cells (Choi et al., 2013; Suan et al., 2015).

A reliable cellular marker to distinguish GC-resident from -nonresident Tfh cells would facilitate efforts to determine whether GC-resident and -nonresident Tfh share a common physiology and function. Higher expression of surface CXCR5 and PD-1 on GCTfh cells generally has been used to discriminate them from other Tfh populations (Crotty, 2011; Tubo et al., 2013; Yusuf et al., 2010). However, this distinction can be difficult, because efficient resolution of CXCR5^{hi} cells requires special adjustments to standard staining methods (Meli and King, 2015; Pepper et al., 2011; Tubo et al., 2013; Yusuf et al., 2010). Moreover, even the strictest definition of GCTfh cells



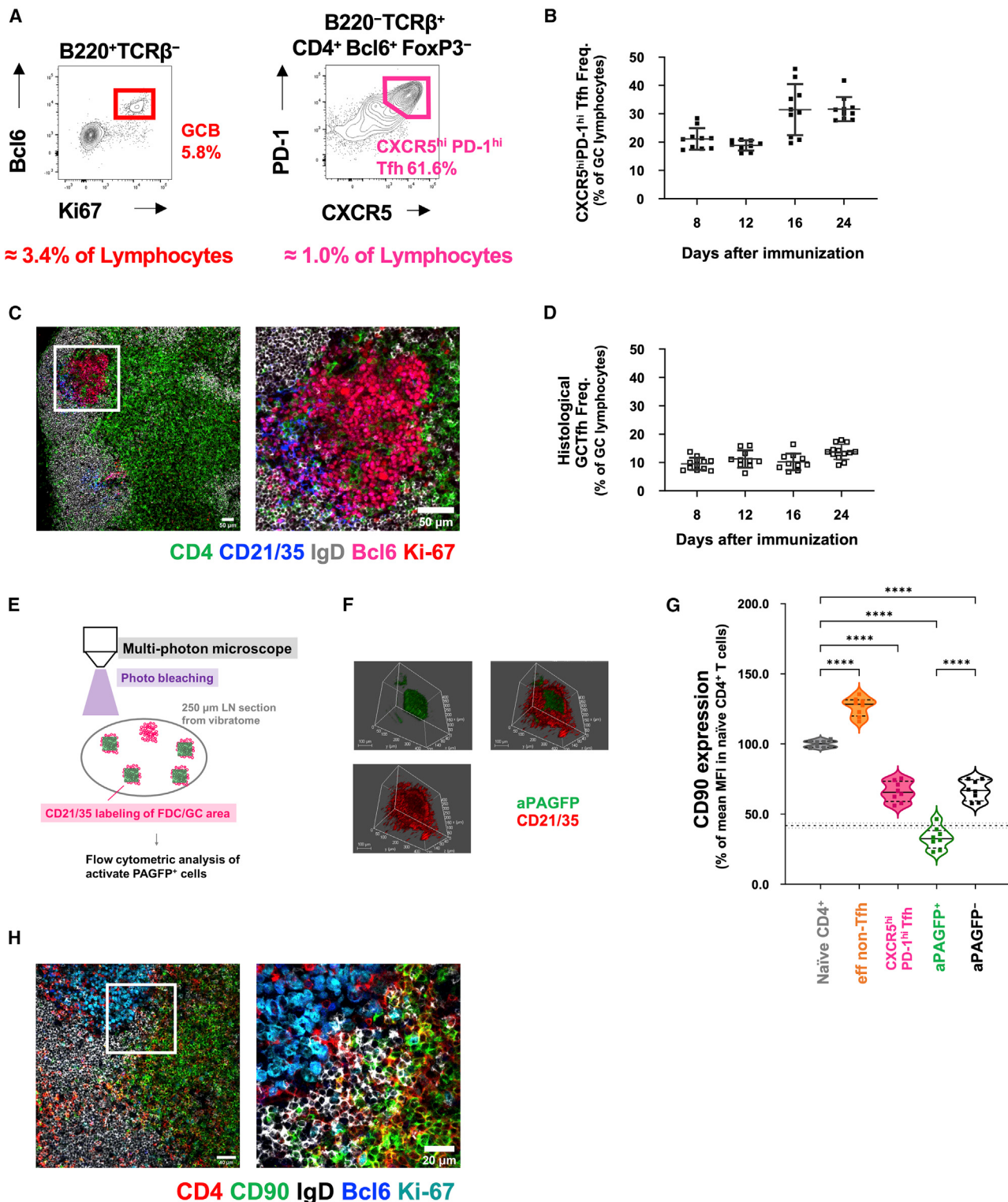


Figure 1. The CXCR5^{hi}PD-1^{hi} GCTfh-cell phenotype comprises mostly GC nonresident Tfh cells

(A-D) B6 mice were footpad-immunized with 20 μ g of NP-Ova+alum.

(A) Flow cytometry contour plots showing the frequencies of GC B cells and CXCR5^{hi}PD-1^{hi} Tfh cells among total pLN lymphocytes 8 days p.i.

(B) Frequencies of CXCR5^{hi}PD-1^{hi} Tfh cells (as determined in A) in individual pLNs 8 to 24 days p.i. (n = 10 at each time point; mean \pm SD).

(C) Representative IF image of GCs, B cell follicles and adjacent T cell zone in pLNs 8 days p.i. The right panel depicts the white boxed area from the left panel, at higher magnification. CD4 (green), CD21/CD35 (blue), IgD (gray), Bcl6 (magenta), Ki-67 (red). Magnification: \times 100 (left), \times 200 (right), scale bars, 50 μ m.

(legend continued on next page)

(CD4⁺FoxP3⁻Bcl6⁺CXCR5^{hi}PD-1^{hi}) is too broad, because such cells constitute $\geq 20\%$ of GC lymphocytes in mice (Cho et al., 2018; Nance et al., 2015; Wu et al., 2015; Yu et al., 2009), in humans (Dan et al., 2019), and in non-human primates (Cirelli et al., 2019; Havenar-Daughton et al., 2016, 2019), whereas more accurate direct histologic analyses reveal that T cells account for only $\approx 10\%$ of GC cellularity (Kelsoe, 1996; Wittenbrink et al., 2011; Wollenberg et al., 2011). Thus, investigating the functions of GCTfh cells and GC-extrinsic Tfh cells would benefit from more precise identification of these subsets.

In this study, we provide a precise definition for GC-resident Tfh cells in primary responses: CXCR5^{hi}PD-1^{hi}CD90^{neg/lo}. These cells were S1pr2⁺, required antigen-specific MHCII⁺ B cells for development, and ceased proliferating after differentiation. In contrast, nonresident GCTfh-like cells were CXCR5^{hi}PD-1^{hi}CD90^{hi}S1pr2⁻, arose in the absence of antigen presentation by B cells and continued proliferating throughout the primary response. Strikingly, these two Tfh populations acquired distinct TCR β repertoires and gene expression profiles, implying their functional heterogeneity and underscoring the importance of dissecting the roles of these discrete cell types in humoral responses.

RESULTS

The CXCR5^{hi}PD-1^{hi} GCTfh phenotype comprises mostly GC nonresident Tfh cells

Flow cytometric analyses and direct histologic observations produce substantially different estimates of GCTfh-cell abundance (Cho et al., 2018; Nance et al., 2015; Wittenbrink et al., 2011; Wollenberg et al., 2011; Wu et al., 2015; Yu et al., 2009). To confirm this discrepancy, we used standard phenotypic definitions for GCB cells (B220⁺Bcl6⁺Ki-67⁺ [Cirelli et al., 2019; Yeh et al., 2018]) and GCTfh cells (CD4⁺FoxP3⁻Bcl6⁺CXCR5^{hi}PD-1^{hi} [Choi et al., 2011; Pepper et al., 2011]) to enumerate by flow cytometry GCB and GCTfh cells in primary GCs elicited by NP-Ova+alum. CXCR5^{hi}PD-1^{hi} GCTfh-phenotype cells constituted $\approx 20\%$ of GC lymphocytes at days 8 and 12 post-immunization (p.i.), rising to $\approx 33\%$ at days 16 and 24 (Figures 1A, 1B, and S1A). In contrast, examination of the same LN tissues by immunofluorescence (IF) microscopy indicated GCTfh cells constituted $\approx 10\%$ of GC lymphocytes from day 8 to 16, rising to $\approx 14\%$ at day 24 (Figures 1C, 1D, and S1B) (Wittenbrink et al., 2011). From the literature and our own experience, we conclude that the Bcl6⁺CXCR5^{hi}PD-1^{hi} phenotype substantially overestimates the size of the true GCTfh-cell compartment. GCTfh cells, defined by their physical location in GCs, are a minor subset of Bcl6⁺CXCR5^{hi}PD-1^{hi} Tfh cells.

To determine a more precise phenotype of GCTfh cells, we turned to mice carrying a photoactivatable green fluorescent protein (PAGFP) transgene (Victora et al., 2010). We immunized PAGFP mice with NP-Ova+alum and 10 days later injected AF594-labeled CD21/CD35 mAb to identify the follicular dendritic cell (FDC) network (Figure 1E). After another 16 h, GCs and FDC networks were readily identified in vibratome sections of draining popliteal LNs (pLNs) (Figure 1F). The central regions of AF594-labeled GCs were then activated using a multi-photon laser and recovered for analysis by flow cytometry. Cells containing activated PAGFP (aPAGFP) comprised both T and B cells within the central GC area (Figures 1F and S1C). In this way, GCB cells were enriched ≈ 8 -fold in the aPAGFP⁺ B cell fraction (75% versus 9%; Figure S1C). aPAGFP⁺ T cells were comparably enriched for Bcl6⁺ cells: 78% of aPAGFP⁺ T cells were Bcl6⁺, compared with only 10% of aPAGFP⁻ T cells (Figure S1C). Almost all aPAGFP⁺Bcl6⁺ CD4 T cells were FoxP3⁻ and exclusively exhibited the CXCR5^{hi}PD-1^{hi} phenotype (Figure S1C).

In addition to the CXCR5 and PD-1 markers for Tfh cells, we previously noted that CD4 T cells in mouse GCs express little or no CD90 (Thy-1) (Zheng et al., 1996). Consequently, we determined levels of CD90 on aPAGFP⁺ GCTfh cells in comparison to resting naive CD4 T cells, all CXCR5^{hi}PD-1^{hi} Tfh cells, and effector non-Tfh cells (eff non-Tfh) (Figures S1A, S1C, and S1D). Compared with resting naive CD4 T cells, the photoactivated GCTfh cells expressed reduced levels of CD90. The MFI of CD90 on aPAGFP⁺ GCTfh was lower than the 10th percentile of CD90 expression in resting naive CD4 T cells (Figure 1G). Loss of CD90 expression was an atypical property of antigen-activated CD4⁺ T cells, as activated eff non-Tfh cells, which expanded in parallel with GCTfh populations (Figure S1D), increased and maintained high CD90 expression throughout the primary response (Figure 1G).

In B6 mice, analysis of the broadest Tfh compartment (CD4⁺Bcl6⁺FoxP3⁻) in day 12 LNs showed that CD90^{neg/lo} Tfh cells were predominantly ($>88\%$) CXCR5^{hi}PD-1^{hi}, whereas only 56% of those cells expressing normal levels of CD90 were CXCR5^{hi}PD-1^{hi} (Figure S1E). Loss of CD90 by Tfh cells correlated with that fraction of GCTfh-phenotype cells resident in GCs, a conclusion confirmed by histologic inspection (Figures 1H and S1F). Whereas CD4⁺CD90^{hi} T cells were detected in paracortex, interfollicular regions, and even in follicles of immunized LNs, CD4⁺ T cells in GCs expressed little or no CD90 (Figures 1H and S1F).

Decreased expression of CD90 in S1pr2-marked GCTfh cells

In a separate approach to identifying GC-resident Tfh cells, we studied primary GC responses in S1pr2^{ERT2Cre-}Rosa26^{lox-stop-lox-tdTomato} (S1pr2-RFP) mice (Shinnakasu

(D) Frequencies of GCTfh cells in individual GCs, as determined by IF analysis ($n = 10$ –12 GCs at each time point; mean \pm SD).

(E–G) PAGFP Tg mice were footpad-immunized with 20 μ g of NP-Ova+alum 11 days prior to analysis.

(E) Diagram of the experimental design.

(F) Representative 3D microscope image showing photoactivation of a region (activated PAGFP, green) within the FDC network (CD21/CD35, red). Original optical magnification: $\times 25$, scale bars 100 μ m.

(G) CD90 MFI of each cell population relative to naive CD4⁺ T cells ($n = 8$; mean \pm SD). The dashed horizontal line indicates the 10th percentile of CD90 expression in naive CD4⁺ T cells (mean \pm SD). ***p ≤ 0.0001 .

(H) B6 mice were immunized as described in (A) for IF analysis 8 days p.i. Representative images show the GC, B cell follicle, T-B border, interfollicular region and nearby T cell zone in the draining pLN. The right panel depicts the white boxed area from the left panel, at higher magnification. CD4 (red), CD90 (green), IgD (gray), Bcl6 (blue), Ki-67 (cyan). Magnification: $\times 200$ (left); $\times 630$ (right), scale bars 40 μ m (left) or 20 μ m (right). Detailed flow cytometry gating strategies are shown in Figure S1.

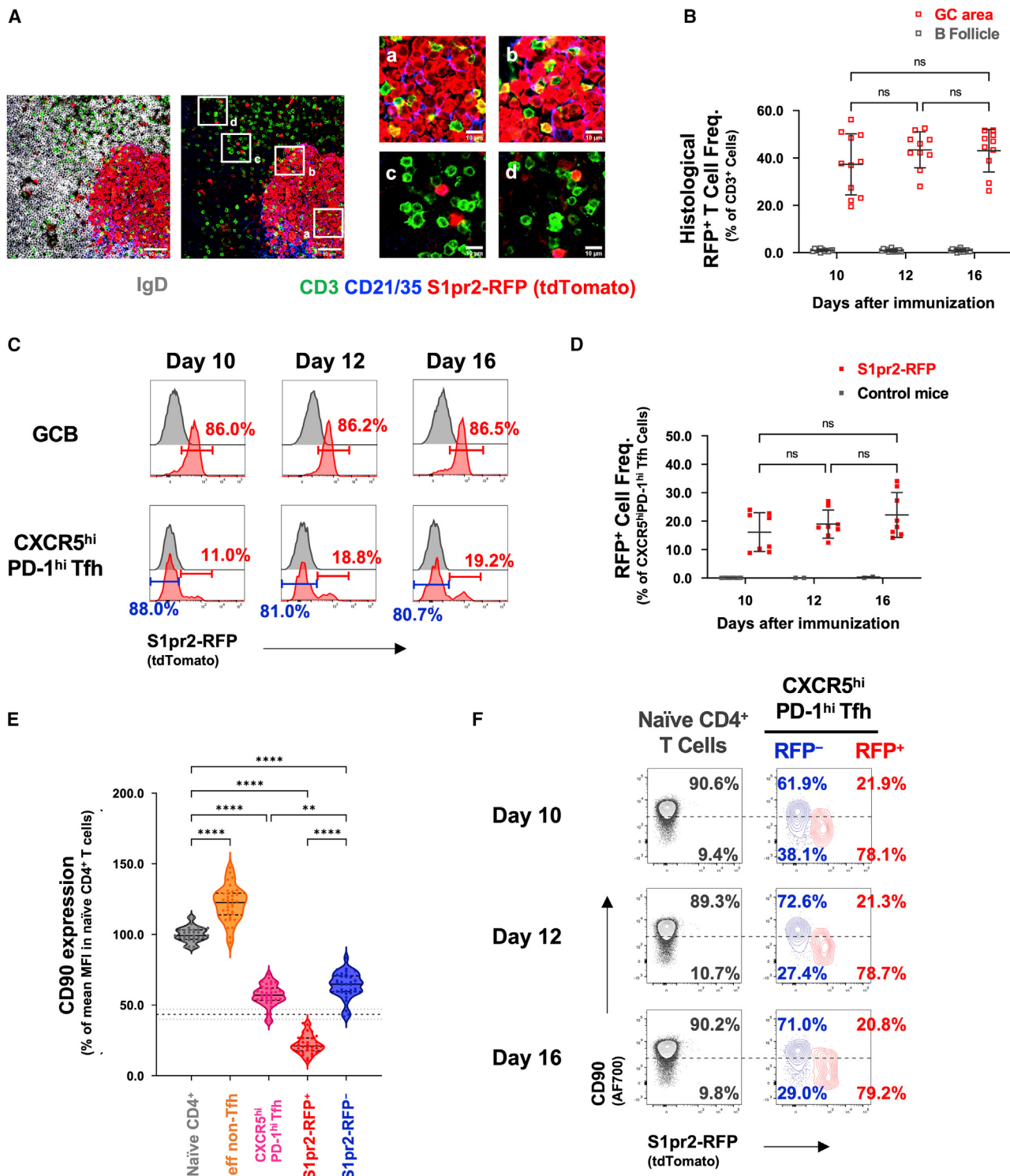


Figure 2. Decreased expression of CD90 in S1pr2-marked GCTfh cells S1pr2-RFP mice were footpad-immunized with 20 µg of NP-Ova+alum and treated with 5 mg tamoxifen (*i.p.*) at days 5–7 p.i.

The draining pLNs were harvested at day 10, 12 and 16 p.i.

(A) IF staining of pLN sections from S1pr2-RFP mice 12 days p.i.; CD3 (green), CD21/CD35 (blue), IgD (gray), tdTomato (red). Magnification: $\times 200$, scale bars 50 µm (left) or 10 µm (right). IgD signal is omitted in the right panels to better visualize T cells in the B follicle.

(B) Frequencies of RFP⁺ Tfh cells in individual GCs or B follicle areas, as determined by IF analysis (n = 10–14 sections from 3 animals at each time point; mean \pm SD).

(legend continued on next page)

et al., 2016). Sphingosine-1-phosphate receptor 2 (S1pr2), a G-protein-coupled receptor, is expressed by both GCB and GCTfh cells and promotes their anatomic retention (Green et al., 2011; Moriyama et al., 2014). To identify GC-resident Tfh cells (i.e., those retained by S1pr2) within the Bcl6⁺ CXCR5^{hi}PD-1^{hi} population, we immunized S1pr2-RFP mice in the footpad with NP-Ova+alum, followed by daily doses of tamoxifen i.p. to induce Cre activity on days 5 to 7 (Figure S2A). Histologic analysis of LN tissue from S1pr2-RFP mice indicated that Tfh cells expressing S1pr2 during the period of tamoxifen treatment were confined to GCs (Figure 2A). Histologic analyses on days 10, 12, and 16 p.i. consistently showed ≈40% of GC-resident CD3⁺ T cells were RFP⁺. In contrast, <1% of CD3⁺ T cells outside of GCs were RFP⁺ over the same period (Figures 2A and 2B). These observations confirmed that S1pr2 is a stringent GCTfh-cell marker. The constancy of RFP⁺ frequencies within GCs implies that GCTfh-cell fate is fixed prior to day 10 p.i., with little or no migration to or from other anatomical sites. The near absence of RFP⁺ T cells in the B cell follicles from days 10–16 p.i. is consistent with no GC-to-GC migration during primary responses (Suan et al., 2015).

More than 85% of GCB-phenotype cells were RFP⁺ on days 10–16 p.i.; in contrast, only 15%–20% of Bcl6⁺CXCR5^{hi}PD-1^{hi} Tfh cells were marked by RFP (Figures 2C, 2D, and S2B). Mature follicular (MF) B and eff non-Tfh cells did not express RFP (Figures S2C and S2D). Regardless of RFP expression, in S1pr2-RFP mice, Bcl6⁺CXCR5^{hi}PD-1^{hi} Tfh cells constituted ≈18% of all GC lymphocytes (GCB + Tfh cells), a frequency identical to that in B6 controls (Figures 1B and S2E). However, RFP⁺ GCTfh cells constituted only 4% of GC cellularity (Figure S2E). Taking the RFP-labeling efficiency into consideration, the size of the S1pr2-expressing GCTfh-cell subset was consistent with the number of GC-resident Tfh cells observed directly by histology (Figure 2B). Therefore, most Bcl6⁺CXCR5^{hi}PD-1^{hi} Tfh cells do not reside in GCs.

In S1pr2-RFP mice, RFP⁺ GCTfh-phenotype cells expressed substantially lower surface CD90 than did naive CD4⁺ T cells, eff non-Tfh or RFP[−] GCTfh-phenotype cells (Figure 2E). Indeed, RFP⁺ and RFP[−] CXCR5^{hi}PD-1^{hi} Tfh subsets could be reliably distinguished by their CD90 expression, with most of the former population expressing CD90 at levels below the 10th percentile of naive CD4 T cells, whereas the great majority of the latter expressed CD90 at levels above the 10th percentile (Figures 2E and 2F). Consequently, we hereafter used this 10th percentile cutoff to define the CD90^{neg/lo} Tfh population in our experiments (Figures 2E, 2F, and S2F). We note that within the RFP[−] GCTfh compartment (Figure 2C), ≈35% of cells were CD90^{neg/lo} on days 10–16 p.i. (Figures 2F and S2G), consistent with the inefficient RFP labeling in GC-resident Tfh cells (Figure 2B). In contrast, >75% of RFP⁺ CXCR5^{hi}PD-1^{hi} Tfh cells were categorized as CD90^{neg/lo} (Figures 2F and S2H).

Primary GCTfh and GCTfh-like cell populations show different dynamics

GCTfh cells have long been considered to be non-dividing, as determined by the lack of Ki-67 expression in GC LZ T cells (Gul-branson-Judge et al., 1997), a key factor in the rationale that limiting numbers of GCTfh cells promotes stringent GCB cell selection (Meyer-Hermann et al., 2006; Wang et al., 2016). This notion was challenged recently by experiments demonstrating that phenotypically defined (CD4⁺CD62^{low}CD44^{hi} Bcl6⁺CXCR5^{hi}PD-1^{hi}) Tfh cells proliferate throughout the GC response (Merkenschlager et al., 2021). To address the issue, we enumerated Ki-67⁺ GC cells in immunized S1pr2-RFP mice on days 10–16 p.i. Unsurprisingly, some 95% of RFP⁺ GCB cells were Ki-67⁺ (Figures 3A and S3A–S3C). In contrast, RFP⁺ GCTfh cells were exclusively Ki-67[−], but ≈26% of RFP[−] GCTfh phenotype cells were Ki-67⁺ (Figures 3A and S3A–S3D). Histological examination of the same LN tissues confirmed that Ki-67⁺ Tfh cells were common in interfollicular regions and B cell follicles but virtually absent from GCs (Figure 3B).

Our histological, photoactivation, and S1pr2-driven labeling experiments demonstrated that even the most stringent previous definition for GCTfh cells (CD4⁺FoxP3[−]Bcl6⁺CXCR5^{hi}PD-1^{hi}) is too broad, because 50%–65% of these cells were not GC residents. Therefore, most prior studies of “GCTfh” cells likely described properties of the larger, GC-nonresident Tfh cell population. To characterize potential functional differences between CD90^{neg/lo} resident GCTfh and CD90^{hi} “GCTfh-like” cells, we followed both populations in LNs after immunization. Cells with the standard CXCR5^{hi}PD-1^{hi} Tfh phenotype were identifiable as early as day 3 p.i. These cells expressed high levels of CD90, and ≈50% were Ki-67⁺, indicating proliferation (Figure 3C). By day 4, before GC B cells could be identified, the CD90^{hi} GCTfh-like population was >80% Ki-67⁺ and had expanded (Figures 3C and S3F). On day 5, ≈10% of the proliferating GCTfh-like population reduced CD90 expression; this shift coincided with the appearance of Bcl6⁺Ki-67⁺ GCB cells and presumably represents the emergence of GC-resident Tfh cells (Figures 3C and S3F). Later, as GCs organized into light and dark zones (Liu et al., 1991), the CD90^{neg/lo} GCTfh compartment became Ki-67[−] (Figure 3C). However, the numbers and frequencies of CD90^{neg/lo} GCTfh and CD90^{hi} GCTfh-like cells both increased through day 8, implying continued recruitment of antigen-specific T cells into both compartments through the peak GCB cell response (Figures 3D and S3G). After the peak GC response, the numbers and frequencies of GCB, CD90^{neg/lo} GCTfh and CD90^{hi} GCTfh-like cells declined, initially with similar kinetics (Figures 3D, S3F, and S3G) but after day 16 the frequencies of GCB and CD90^{neg/lo} GCTfh cells stabilized, whereas CD90^{hi} GCTfh-like cell frequencies continued to decrease (Figures 3C and 3D). Consequently, over time, CD90^{neg/lo} GCTfh cells increased their representation among the broader Bcl6⁺CXCR5^{hi}PD-1^{hi} population (Figures 3C and S3H). Similar

(C and D) (C) Representative flow histogram plots and (D) dot plots showing the frequencies of RFP⁺ Tfh cells ($n = 8$ at each time point; mean \pm SD). (E) CD90 expression in each cell population relative to naive CD4⁺ T cells ($n = 34$; mean \pm SD). The dashed line indicates the 10th percentile of CD90 expression in naive CD4⁺ T cells (mean \pm S.D.). (F) Representative flow cytometry contour plots showing the frequencies of naive (gray), RFP[−] Tfh (blue) and RFP⁺ GCTfh (red) cells above (CD90^{hi}) or below (CD90^{neg/lo}) the 10th percentile of CD90 expression in naive CD4 T cells (dashed line). Each symbol represents an individual mouse. Data were pooled from ≥ 2 independent experiments. Statistical significance was measured using ordinary ANOVA followed by Tukey's post-test (E; ** $p < 0.01$; *** $p < 0.0001$).

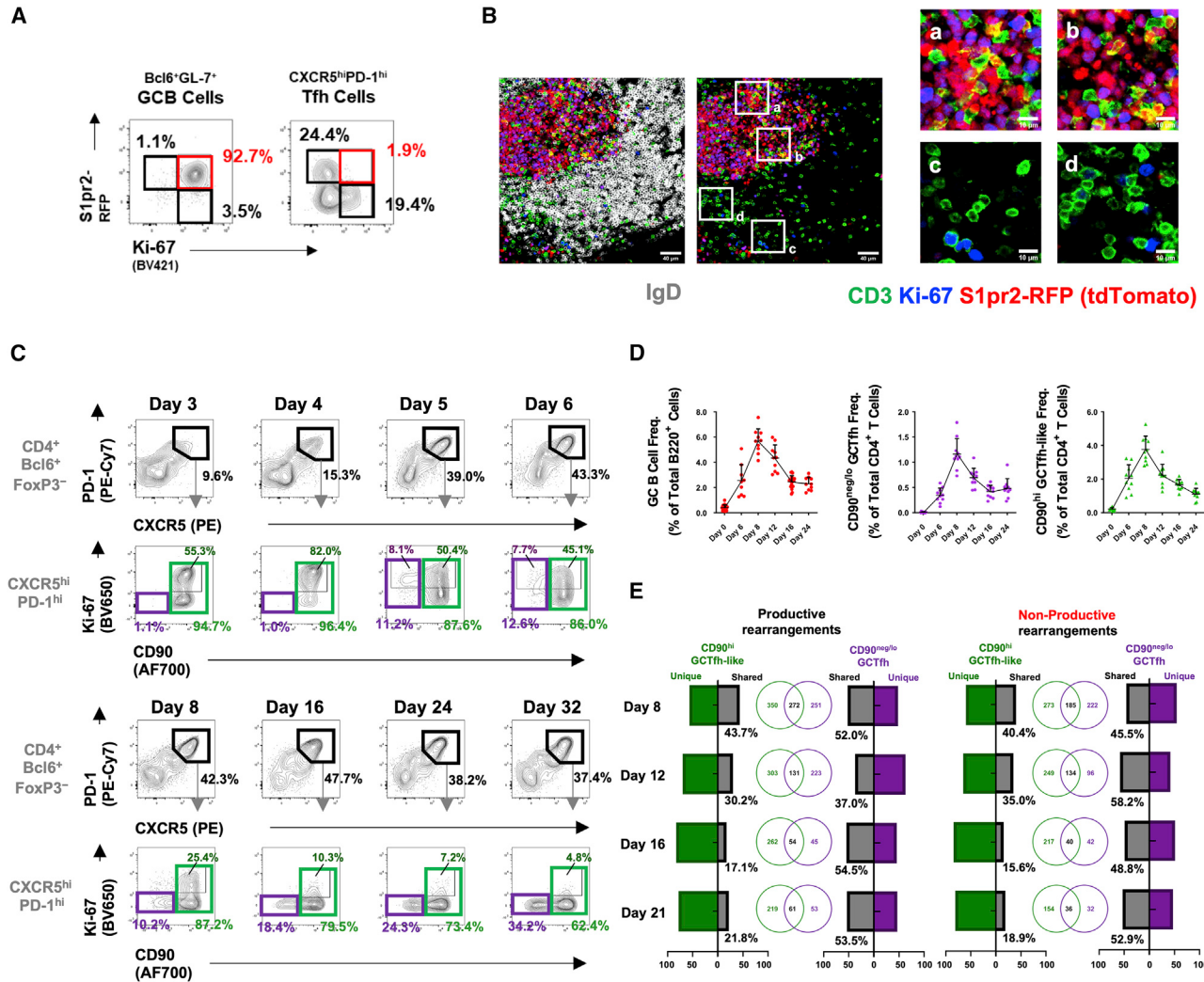


Figure 3. GCTfh and GCTfh-like cells follow different dynamics in primary responses

(A and B) S1pr2-RFP mice were immunized and treated as described in Figure S2A.

(A) Representative flow cytometry contour plots show the frequencies of RFP⁺Ki-67⁺ GC B cells and RFP⁺Ki-67⁻ Tfh cells.

(B) IF analysis of pLN from S1pr2-RFP mice 12 days p.i.; CD3 (green), IgD (gray), Ki-67 (blue), tdTomato (red). Magnification: $\times 200$, scale bars indicate 50 μ m (left) or 10 μ m (right). IgD signal is omitted in the right panels to better visualize T cells in the B follicle.

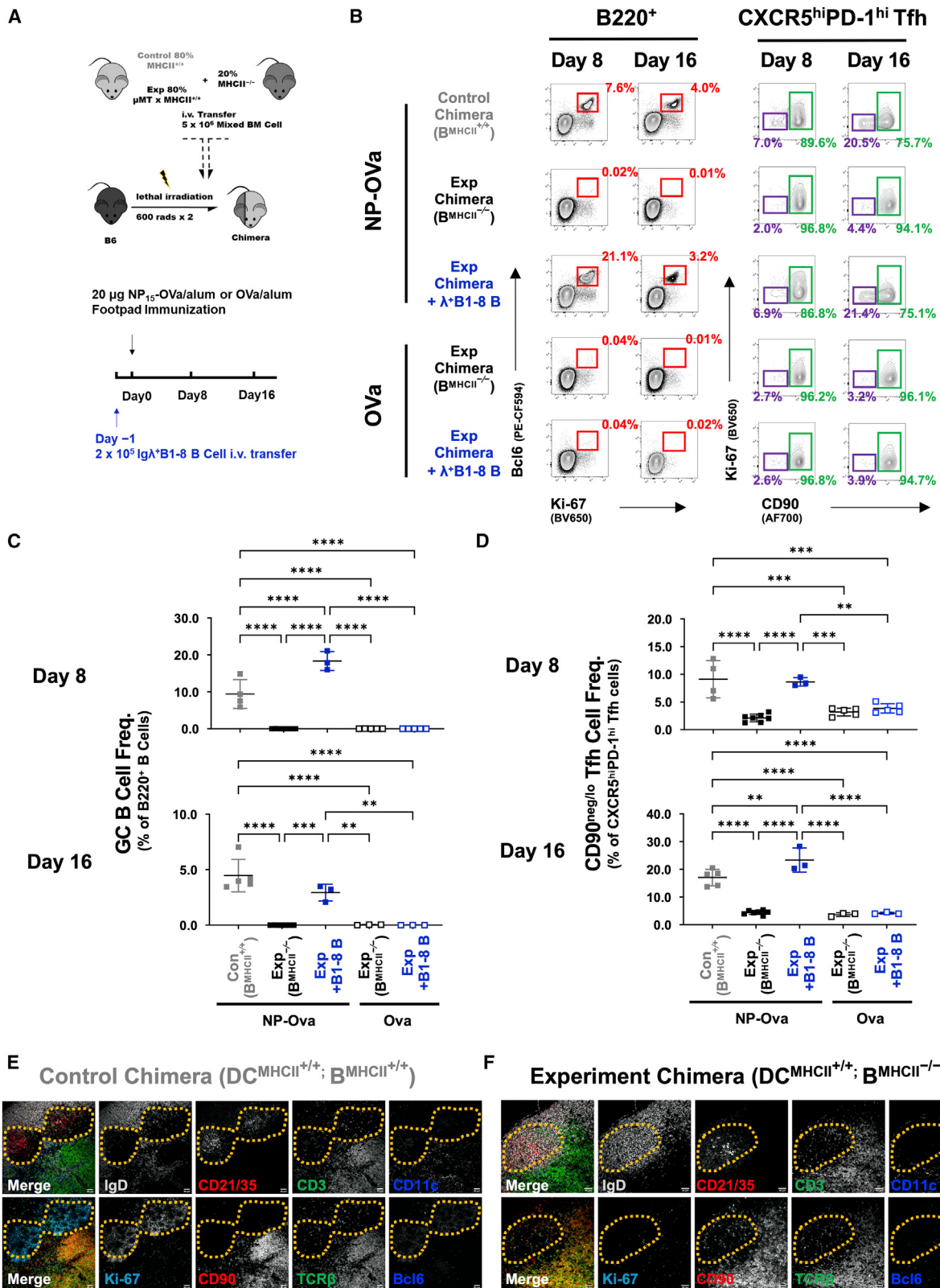
(C) Flow cytometry plots indicating the frequencies of CXCR5^{hi}PD-1^{hi} Tfh cells among TCR β^+ CD4⁺Bcl6⁺FoxP3⁻ cells; and the frequencies of CD90^{neg/lo} GCTfh (CD90^{neg/lo}; purple), proliferating GCTfh-like (CD90^{hi}Ki-67⁺; dark green) or total CD90^{hi} GCTfh-like (light green) populations among all CXCR5^{hi}PD-1^{hi} Tfh cells.

(D) The population kinetics of GCB cells (left), CD90^{neg/lo} GCTfh cells (center), and CD90^{hi} GCTfh-like cells (right) after immunization ($n = 10$ at each time point; mean \pm SD).

(E) FoxP3^{EGFP} mice were footpad-immunized with 20 μ g of NP-Ova+alum and pLN cells were analyzed at indicated time points. CD90^{neg/lo} GCTfh (purple) and CD90^{hi} GCTfh-like cells (green) were sorted from the same pLN and were subjected to high-throughput TCR β sequencing. Venn diagrams depict the numbers and bar charts the frequencies of unique and shared VDJ rearrangements. TCR β sequencing data represent one of two independent experiments with similar results. Gating strategies are shown in Figure S7A.

population dynamics of CD90^{neg/lo} GCTfh and CD90^{hi} GCTfh-like cells were elicited by multiple antigens, including *B. anthracis* protective antigen and influenza H1 hemagglutinin (Figure S3H). Taken together, CD90^{neg/lo} GCTfh cells are non-proliferative, but the proportion of this population among all Bcl6⁺CXCR5^{hi}PD-1^{hi} Tfh cells increases as the GC reaction wanes, suggesting local stability whereas CD90^{hi} GCTfh-like cells migrate or die.

To determine whether CD90^{neg/lo} GCTfh cells are unique to transient GCs elicited by primary immunization, we analyzed the composition of constitutive GCs in Peyer's patches (PPs) of B6 mice (Figures S3I–S3L). CD90^{neg/lo} GCTfh cells were as abundant in PPs as in primary GCs elicited by NP-Ova (Figures 3C and S3K); in PPs, CD90^{neg/lo} GCTfh cells constituted $\approx 18\%$ of the Bcl6⁺CXCR5^{hi}PD-1^{hi} Tfh cell population (Figure S3M). Notably, CXCR5^{hi}PD-1^{hi} Tfh cells represented $\approx 25\%$ of GC lymphocytes,



whereas CD90^{neg/lo} GCTfh cells constituted only ≈5% (Figure S3N). Thus, like the GC responses elicited by primary immunization, chronic GC responses driven by dietary and environmental antigens support CD90^{neg/lo} GCTfh cells.

To investigate the clonal origins of CD90^{neg/lo} GCTfh and CD90^{hi} GCTfh-like cells, we isolated both populations from a common LN and used high-throughput sequencing to recover the Tcrβ rearrangements present in each (Carlson et al., 2013). From pLNs at days 8, 12, 16, and 21 p.i., we obtained 6,179 and 8,977 Tcrβ VDJ templates from CD90^{neg/lo} GCTfh and CD90^{hi} GCTfh-like cells, respectively (Figure S3O). Among these, 2,902 and 1,877 unique rearrangements were found in each compartment. At day 8, there was substantial overlap in the Tcrβ rearrangements expressed by CD90^{neg/lo} GCTfh and CD90^{hi} GCTfh-like cells, with ≈44% of all Tcrβ rearrangements from CD90^{hi} GCTfh-like cells being shared with CD90^{neg/lo} GCTfh cells (Figure 3E). Thereafter, sharing diminished significantly, such that by day 21, only 22% of Tcrβ rearrangements were shared. Whereas about half of the Tcrβ rearrangements in CD90^{neg/lo} GCTfh cells were always shared with CD90^{hi} GCTfh-like cells over the course of the response, the converse was not true (Figures 3E and S3O). Similar patterns of divergence were observed for both productive and non-productive Tcrβ rearrangements, implying discordant selection/expansion between the two populations (Figure 3E).

Differentiation and maintenance of CD90^{neg/lo} GCTfh cells requires antigen-specific, MHCII⁺ B cells

Although Tfh cell commitment occurs within the first few rounds of cell division after activation by antigen, Tfh cell differentiation is a process that includes stepwise priming by DCs and cognate interaction with B cells at the border of T- and B cell zones (Choi et al., 2013; DiToro et al., 2018; Tubo et al., 2013). Given that CD90^{hi} GCTfh-like and CD90^{neg/lo} GCTfh cells extensively shared Tcrβ rearrangements early but not late after immunization (Figures 3E and S3O) and that differentiation of the CD90^{neg/lo} GCTfh-cell subset coincided with the appearance of GCB cells, we hypothesized that CD90^{neg/lo} GCTfh-cell differentiation requires continued B cell interaction whereas the CD90^{hi} GCTfh-like population does not. To test this hypothesis, we generated experimental mixed BM chimeras in which all B cells (but only 20% of DCs) were MHCII-deficient; in isogenic control chimeras, B cells expressed MHCII normally (Figure 4A). Finally, IgD⁺Igλ⁺ B1-8i NP-specific B cells (Sonoda et al., 1997) were transferred *i.v.* to experimental chimeras one day before immunization with NP-Ova or Ova to provide cohorts of MHCII-sufficient and antigen-specific (NP-Ova) or unspecific (Ova) B cells (Figure 4A).

After immunization, control chimeras generated potent GC responses, but in experimental chimeras with only MHCII-deficient B cells, no GCB cells were generated (Figures 4B and 4C). Transfer of B1-8i B cells fully restored GCB responses in mice immunized with NP-Ova, but not with Ova alone (Figures 4B and 4C). In concert with the presence or absence of GCB cells, we observed significant changes in the frequencies of CD90^{neg/lo} GCTfh cells within the CXCR5^{hi}PD-1^{hi} Tfh compartment. In control chimeras, CD90^{neg/lo} GCTfh cells represented 9%–17% of all CXCR5^{hi}PD-1^{hi} Tfh cells on days 8 and 16 p.i. Similar frequencies were observed in experimental chimeras given B1-8i cells and immunized with NP-Ova. In contrast, in both experimental chimeras or experimental chimeras given B1-8i cells and immunized with Ova, CD90^{neg/lo} GCTfh cells constituted just 2%–3% of CXCR5^{hi}PD-1^{hi} Tfh cells on days 8 and 16 (Figures 4B, 4D, and S4A–S4D). We note that Tfh cells in non-responding experimental chimeras expressed lower levels of PD-1 compared with controls (Figure S4A). Importantly, the presence or absence of MHCII-sufficient B cells did not affect the frequencies of eff non-Tfh cells (Figure S4B).

Histologic examination of pLNs from control and experimental chimeras (Figures 4E–4F) confirmed the flow cytometry results. Eight days after immunization, control chimeras generated Ki-67⁺Bcl6⁺ GCs within the CD21/CD35⁺ reticula of FDC in B cell follicles (Figure 4E). In contrast, whereas typical follicles and FDC networks were present in experimental chimeras with MHCII-deficient B cells, no GCs were generated (Figure 4F). In control chimeras, CD90^{neg/lo} GCTfh cells were observed in GCs, whereas CD90^{hi} GCTfh-like cells were present in the interfollicular regions and at the intersection of T cell zones and follicles (Figure 4E; compared with Figure 1H). However, in experimental chimeras, CD3⁺CD90^{hi} or TCRβ⁺CD90^{hi} Tfh cells were uniformly distributed over the B cell follicle (Figure 4F). We conclude that antigen-specific B cells, presumably as cognate partners, are necessary for the differentiation of CD90^{neg/lo} GCTfh cells, whereas CD90^{hi} GCTfh-like cells readily develop when DCs are the exclusive antigen-presenting cells. Cognate T:B interaction provides a specific cue for CD90^{neg/lo} GCTfh-cell development.

To define the window during which antigen-specific, MHCII-sufficient B cells confer the signal for CD90^{neg/lo} GCTfh-cell differentiation, we transferred Mb1^{Cre}xDTR^{LSL} B cells into chimeric mice in which all other B cells (but not DCs) were MHCII^{−/−} and incapable of antigen presentation (Figure 4A). We then immunized the mice and administered diphtheria toxin (DTx) at various intervals to kill antigen-presenting B cells (Figures 5A and S4E). DTx administration began either (1) on the day of immunization

Figure 4. Differentiation and maintenance of CD90^{neg/lo} GCTfh cells require antigen-specific, MHCII⁺ B cells

(A) Diagram of the experimental design.
(B) Representative flow cytometry contour plots depicting the frequencies of B220⁺Bcl6⁺Ki-67⁺ GCB cells among B220⁺ cells (red; left panel) and of CD90^{neg/lo} Ki-67[−] (CD90^{neg/lo} GCTfh; purple) or CD90^{hi} GCTfh-like (green) cells among all CXCR5^{hi}PD-1^{hi} Tfh cells in pLNs at days 8 and 16 p.i.
(C and D) Frequencies of (C) GCB cells among total B220⁺ B cells and (D) CD90^{neg/lo} GCTfh cells among CXCR5^{hi}PD-1^{hi} Tfh cells at indicated time points ($n = 3$ –8 at each time point; mean \pm SD). Each symbol represents an individual mouse; data were pooled from at least two independent experiments. Statistical significance was measured using ordinary ANOVA followed by Tukey's post-test (** $p < 0.01$; *** $p < 0.001$).
(E and F) Representative images showing IF analysis of serial sections from the LNs of (E) a control chimera (DC^{MHCII^{+/+}}; B^{MHCII^{+/+}}) and (F) an experimental chimera (DC^{MHCII^{+/+}}; B^{MHCII^{−/−}}). The far left panel in each series depicts the merged signals from the subsequent four panels. Top row: IgD (gray), CD21/35 (red), CD3 (green), CD11c (blue). Bottom row: Ki-67 (cyan), CD90 (red), TCRβ (green), Bcl6 (blue). Dashed yellow lines circumscribe the GC (E) or FDC network (F). Magnification: $\times 200$, scale bars 40 μ m. Data represent one of two independent experiments with similar results.

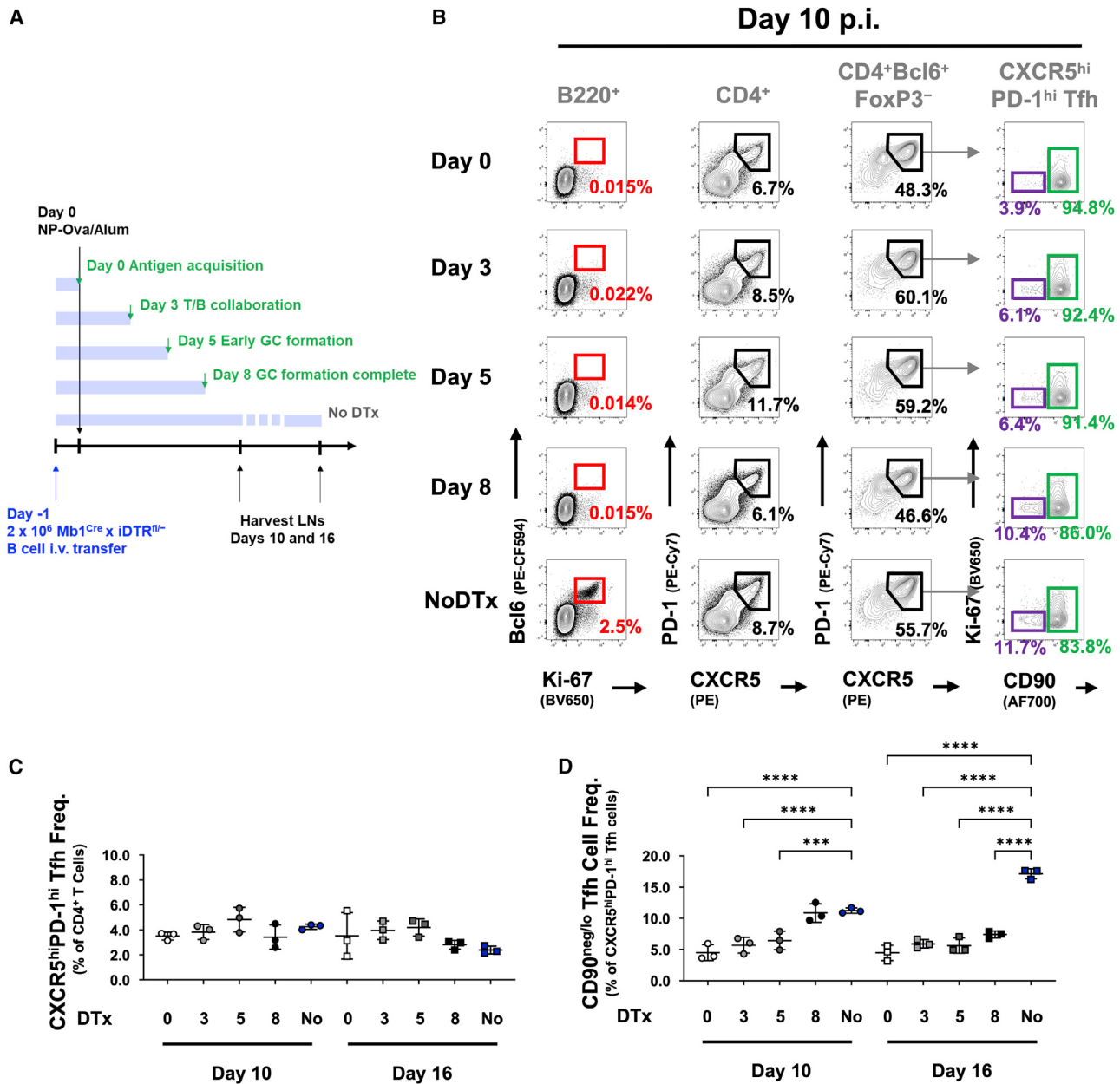


Figure 5. CD90^{neg/lo} GCTfh-cell differentiation requires B cells to present cognate pMHCII until GCs completely coalesce

(A) Diagram of the experimental design. Chimeric mice were generated as in Figure 4A. 2×10^6 MB1^{Cre} x iDTR^{SL} mice were i.v. transferred 1 day prior to immunization. DTx was i.p. injected starting at indicated time points. Draining pLNs were harvested at day 10 or 16 p.i.

(B) Representative flow cytometry contour plots depicting the frequencies of B220⁺Bcl6⁺Ki-67⁺ GCB cells (red; left column), CD4⁺CXCR5^{hi}PD-1^{hi} Tfh cells (second column), CD4⁺FoxP3⁻Bcl6⁺CXCR5^{hi}PD-1^{hi} Tfh cells (third column) and CD90^{neg/lo} Ki-67⁻ (CD90^{neg/lo} GCTfh; purple, fourth column) and CD90^{hi} GCTfh-like (green, fourth column) populations in pLNs harvested from each group of chimeras at day 10 p.i.

(C and D) Frequencies of (C) CXCR5^{hi}PD-1^{hi} Tfh cells among total CD4⁺ T cells and (D) CD90^{neg/lo} GCTfh cells among CXCR5^{hi}PD-1^{hi} Tfh cells at indicated time points ($n = 3$ at each time point; mean \pm SD). Each symbol represents an individual mouse; results were pooled from at least two independent experiments. Statistical significance was determined using ordinary ANOVA followed by Tukey's post-test (**p < 0.01; ***p < 0.001).

(d0) to block any cognate T:B interaction; (2) during early T/B collaboration (d3); (3) at the initiation of GC formation (d5), or (4) after GC organization was complete (d8) (Crotty, 2019). Once initiated, i.p. injections of DTx occurred every other day to maintain effective serum concentrations of DTx (Meredith et al., 2012). In all cohorts, GCB, CD90^{neg/lo} GCTfh, and

CD90^{hi} GCTfh-like cells were enumerated at days 10 and 16 p.i. (Figure 5A).

DTx injection effectively depleted all transferred B cells, ending any capacity for humoral responses and abrogating GCs. Regardless of when DTx administration began, GCB cells were completely absent in all treated mice (Figure S4F).

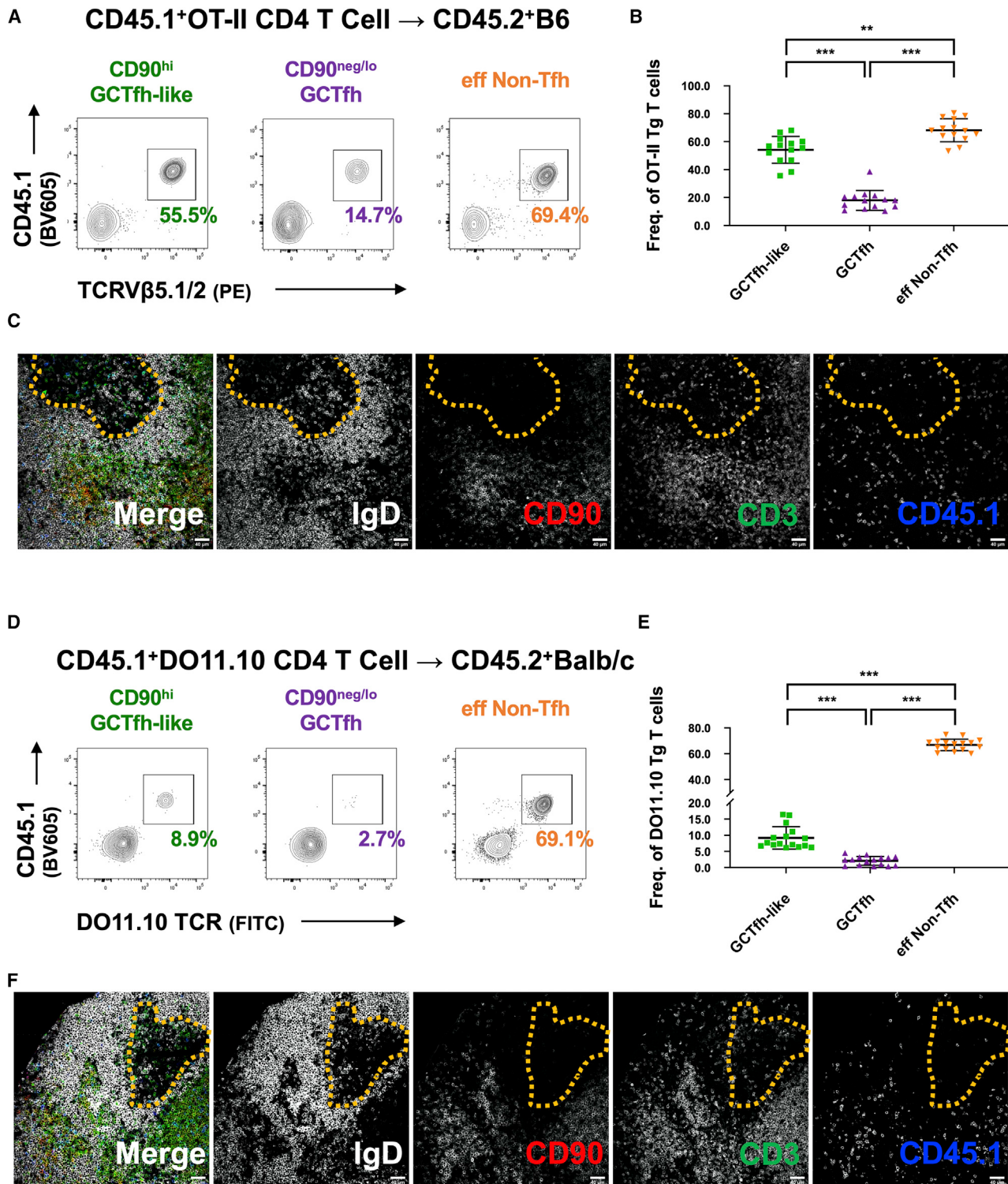


Figure 6. TCR influences the likelihood of CD90^{neg/lo} GCTfh-cell differentiation

CD4⁺ T cells from (A–C) CD45.1⁺ OT-II or (D–F) CD45.1⁺ DO11.10 mice were adoptively transferred into B6 or BALB/c mice. Hosts were subsequently footpad-immunized with 20 µg of NP-Ova+alum. Draining pLNs were analyzed at day 8 p.i.

(A) Representative flow cytometry contour plots and (B) summary graph depicting the frequencies of CD45.1⁺TCRV β 5⁺ transferred OT-II cells among CD90^{hi} GCTfh-like, GCTfh and eff non-Tfh cells ($n = 14$; mean \pm SD).

(C) Representative IF images showing cryostat sections from draining pLNs.

However, B cell depletion at any time point did not affect the size of the total CXCR5^{hi}PD-1^{hi} Tfh cell population present on days 10 and 16 p.i. (Figures 5B and 5C). In contrast, depleting GCB cells significantly reduced the size of the CD90^{neg/lo} GCTfh compartment. DTx given in the early phases of GC response (day 0, 3, or 5) reduced CD90^{neg/lo} GCTfh-cell frequencies 2- to 3-fold on day 10 and 3- to 4-fold on day 16 (Figure 5D). Treatment with DTx beginning at day 8, after GCs become fully organized, did not affect CD90^{neg/lo} GCTfh-cell frequencies on day 10, but on day 16, CD90^{neg/lo} GCTfh-cell frequencies fell to half that of controls (Figures 5B, 5D, and S4G–S4I). This loss after GC organization suggests that sustained cognate T:B interaction is necessary to maintain CD90^{neg/lo} GCTfh populations. DTx-mediated B cell depletion at any time did not affect the frequencies of eff non-Tfh cells (Figure S4J).

Continued proliferation of CD90^{hi} GCTfh-like cells is DC dependent

The dispensability of B cells for robust responses of CXCR5^{hi}PD-1^{hi}CD90^{hi} GCTfh-like cells implies that conventional DCs (cDCs) alone are sufficient for the differentiation and maintenance of this T cell population. To test this hypothesis, we generated Zbtb46-DTR BM chimeras to restrict DTR expression to cDCs (Meredith et al., 2012). We immunized these animals with NP-Ova+alum, and then depleted the cDC compartment by DTx injection on day 7 p.i., after GC organization was complete (Figure S5A). On days 8, 12, and 16 p.i., we enumerated and characterized MHCII^{hi}CD11c⁺ migratory cDCs (mDCs) and MHCII⁺CD11c^{hi} LN-resident cDCs (rDCs), along with GCB, CD90^{neg/lo} GCTfh, and CD90^{hi} GCTfh-like cells (Figures S5B–S5J).

Whereas DTx injection effectively reduced both mDC and rDC frequencies (Figures S5B, S5E, and S3F), the frequencies of GCB (Figures S5C and S5G) and CD90^{neg/lo} GCTfh cells (Figures S5D and S5H) were unaffected. Frequencies of CD90^{hi} GCTfh-like cells were also unchanged (Figures S5D and S5I), but cDC ablation significantly reduced CD90^{hi} GCTfh-like cell proliferation at days 12 and 16, as measured by lower frequencies of Ki-67⁺CD90^{hi} cells (Figures S5D and S5J). We conclude that Tfh cell proliferation in the CD90^{hi} compartment is driven by cognate interaction with antigen-presenting cDCs, an observation that might explain the diverging TCR β repertoires of CD90^{hi} GCTfh-like and CD90^{lo} GCTfh-cell populations.

The influence of antigen receptors on CD90^{neg/lo} GCTfh-cell differentiation

The fact that the TCR repertoires of CD90^{neg/lo} GCTfh and CD90^{hi} GCTfh-like cells diverged over time (Figure 3E) suggests that not all antigen-specific TCRs equally support GCTfh-cell differentiation. To investigate the potential impact of individual TCRs on CD4⁺ T cell fates, we adoptively transferred CD4⁺ T cells from CD45.1⁺ OT-II or DO11.10 TCR transgenic mice

into naive CD45.2⁺ B6 or BALB/c hosts, respectively. The OT-II and DO11.10 TCRs are specific for the Ova_{323–339} peptide presented on I-A^b or I-A^d (Robertson et al., 2000). We then immunized recipient mice with NP-Ova and analyzed draining pLNs by flow cytometry on day 8 p.i. to determine the participation of OT-II or DO11.10 T cells in the CD90^{neg/lo} GCTfh, CD90^{hi} GCTfh-like, and eff non-Tfh cell compartments.

Transferred OT-II T cells were capable of differentiating into GCTfh, GCTfh-like and eff non-Tfh cells in the presence of endogenous competitors; however, the frequency of OT-II cells in each subset varied significantly (Figures 6A and 6B). Although the OT-II cells constituted 70% and 50% of eff non-Tfh and GCTfh-like subsets, respectively, only about 15% of GCTfh cells were OT-II T cells (Figures 6A and 6B). Histology confirmed that most of the transferred OT-II T cells expressed CD90 and were located at the T-B border, in B cell follicles or in T cell zones (Figure 6C). The propensity toward non-Tfh fates was even more extreme in DO11.10 transgenic T cells transferred to BALB/c recipients: DO11.10 T cells constituted 67% of the eff non-Tfh subset, but only 10% and 2% of the GCTfh-like and GCTfh populations, respectively (Figures 6D–6F). We conclude that these commonly used transgenic TCRs are better suited for studying GCTfh-like and eff non-Tfh cell responses than for probing the physiology of GCTfh cells.

B cells carrying low-affinity BCRs are fully capable of T-dependent immune responses (Dal Porto et al., 1998), but it is unclear whether BCR affinity affects GCTfh-cell development. To address this question, we used NP-conjugated human serum albumin (NP-HSA)+alum to immunize B6.H50G μ transgenic mice, which express an IgM BCR that, with the λ 1 light chain, binds the NP hapten with an association constant (K_a) of 1.2×10^5 M⁻¹ (Dal Porto et al., 1998). We also immunized a second cohort of B6.H50G μ mice that had received 1×10^5 NP-specific λ^+ B cells from B1-8i mice ($K_a = 1.0 \times 10^6$ M⁻¹ (Dal Porto et al., 1998; Sonoda et al., 1997)) to determine whether higher BCR affinity affects GCTfh-cell differentiation. As expected, immunized B6.H50G μ mice that had received B1-8i B cells supported ≥ 5 -fold larger GCB cell responses than immunized control B6.H50G μ mice (Figures S6A–S6D). Despite the significant increases in GCB cell responses, the frequencies of total CXCR5^{hi}PD-1^{hi} Tfh and CD90^{hi} GCTfh-like cells were comparable in both cohorts (Figures S6A and S6E). In contrast, CD90^{neg/lo} GCTfh-cell frequencies and numbers were significantly increased in B6.H50G μ mice supplemented with B1-8i B cells (Figure S6F). Thus, higher BCR affinity promotes CD90^{neg/lo} GCTfh-cell differentiation but has limited effect on CD90^{hi} GCTfh-like cell populations.

Transcriptional profiling implies functional divergence of CD90^{neg/lo} GCTfh and CD90^{hi} GCTfh-like cells

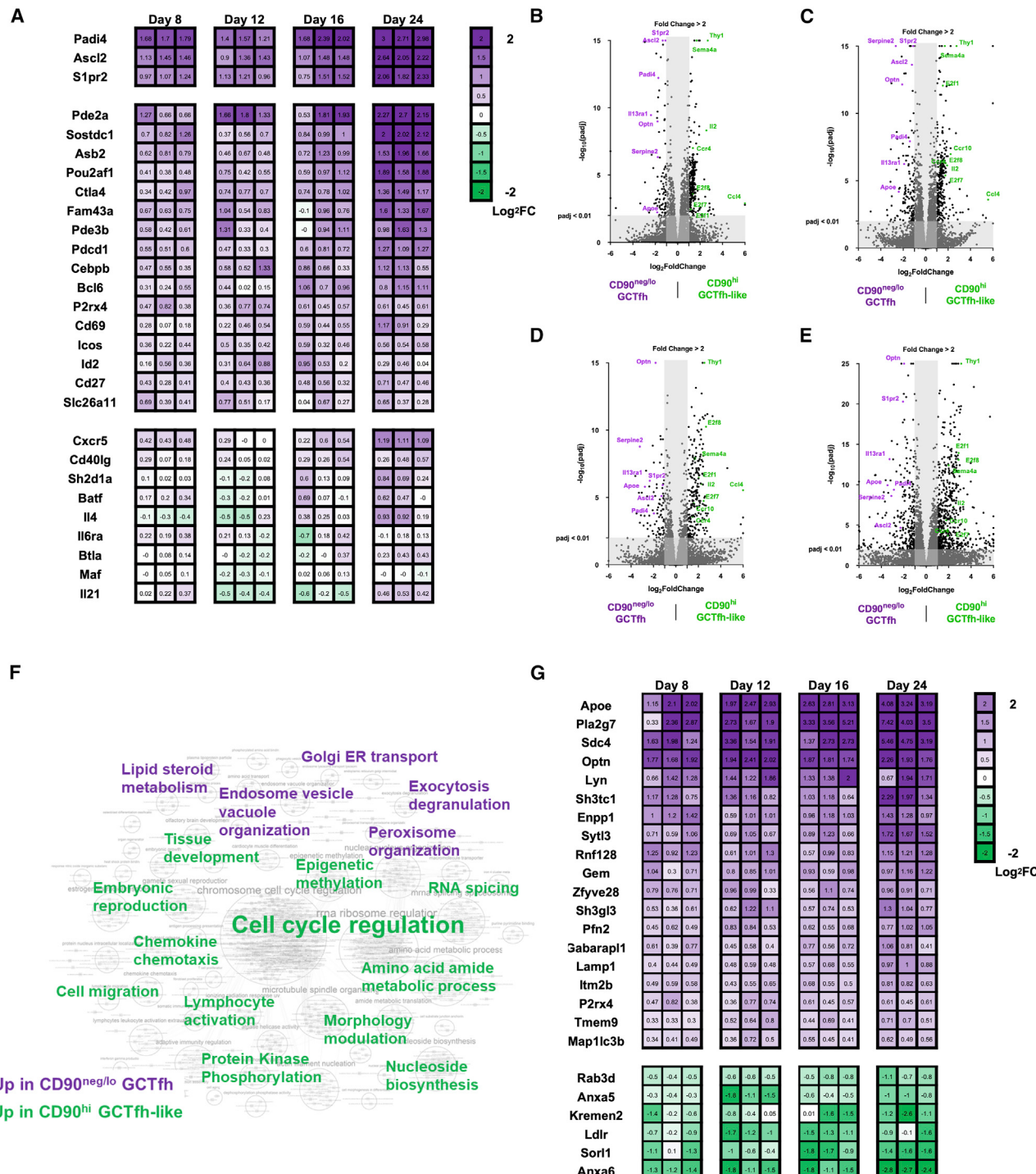
To identify functional differences between CD90^{neg/lo} GCTfh and CD90^{hi} GCTfh-like cells, we performed RNA sequencing

(D and E) (D) Representative flow cytometry contour plots and (E) summary graph depicting the frequencies of CD45.1⁺DO11.10Tg⁺ transferred cells among CD90^{hi} GCTfh-like, GCTfh and eff non-Tfh cells ($n = 16$; mean \pm SD).

(F) Representative IF images showing cryostat sections from draining pLNs.

(B and E) Each symbol represents an individual mouse LN. Results were pooled from at least two independent experiments. Statistical significance was measured using ordinary ANOVA followed by Tukey's post-test (**p < 0.01; ***p < 0.001).

(C and F) The far left panel depicts the merged signals from the subsequent four panels. IgD (gray), CD90 (red), CD3 (green), CD45.1 (blue). Dashed yellow lines circumscribe the GC region. Magnification: $\times 200$, scale bars, 40 μ m.

**Figure 7. Transcriptional profiling implies functional divergence of CD90^{neg/lo} GCTfh and CD90^{hi} GCTfh-like cells**

FoxP3^{EGFP} mice were footpad-immunized with 20 µg of NP-Ova+alum. Draining pLNs were harvested at days 8, 12, 16, and 24 p.i. CD90^{neg/lo} GCTfh (purple) and CD90^{hi} (green) GCTfh-like cells were sorted from the same pLN and were subjected to ultra-low RNA sequencing. Detailed gating strategies are shown in Figure S7A. RNA was extracted and then subjected to library preparation and sequencing. Differential gene expression was performed in R by DESeq2. (A) Heatmap graph showing the fold-change of Tfh-related gene expression in CD90^{neg/lo} GCTfh over CD90^{hi} GCTfh-like cells in each individual pLN. Numbers indicate the log₂ fold-change in gene expression (n = 3 at each time point). (B–E) Volcano plots depicting genes up- or downregulated with fold-change ≥ 2 and adjusted p value < 0.01 in CD90^{neg/lo} GCTfh cells relative to CD90^{hi} GCTfh-like cells at (B) day 8, (C) day 12, (D) day 16 or (E) day 24.

(legend continued on next page)

(RNA-seq) on both populations, together with eff non-Tfh and T_{FR} cells isolated from the same LN of FoxP3^{EGFP} mice (Haribhai et al., 2007), at 8, 12, 16, and 24 days p.i. (Figure S7A). Transcriptomes for each T cell population were obtained by deep-sequencing cDNA libraries. Transcriptional profiles of CD90^{neg/lo} GCTfh cells relative to CD90^{hi} GCTfh-like, eff non-Tfh and T_{FR} cells were compared by principal component analysis of each cohort and grouping d8 and d12 (Figure S7B), or d16 and d24 samples (Figure S7C). The transcriptome of each T cell group was clearly distinct: eff non-Tfh and T_{FR} cells displayed higher intra-subset variability than did the CD90^{neg/lo} GCTfh and CD90^{hi} GCTfh-like cohorts (Figures S7B and S7C). Despite shared clonal origins for many CD90^{neg/lo} GCTfh and CD90^{hi} GCTfh-like cells (Figure 3E), z-score normalized heatmap analysis revealed significant differences ($p < 0.05$ and ≥ 2 -fold-change) in gene expression between these groups (Figure S7D). Compared with CD90^{hi} GCTfh-like cells, the transcriptome of CD90^{neg/lo} GCTfh cells was significantly enriched for the Tfh-related genes *Ascl2*, *Padi4*, and *S1pr2* (Liu et al., 2014; Moriyama et al., 2014; Wing et al., 2017) at every time point (Figures 7A–7E). Other Tfh-related genes, including *Axb2*, *Bcl6*, *Cd27*, *Cd69*, *Cebpb*, *Ctla4*, *Fam43a*, *Icos*, *Id2*, *P2rx4*, *Pdcdf1*, *Pde2a*, *Pde3b*, *Pou2af1*, *Slc26a11*, and *Sostdc1* (Choi et al., 2015; Wing et al., 2017), were significantly elevated ($p < 0.05$) in the CD90^{neg/lo} GCTfh compartment but occasionally did not meet the ≥ 2 -fold threshold at some time points (Figure 7A). Still, other Tfh-related genes, including *Batf*, *Btla*, *Cd40lg*, *Cxcr5*, *Il4*, *Il6ra*, *Il21*, *Maf*, and *Sh2d1a* (Choi et al., 2015; Moriyama et al., 2014; Wing et al., 2017), were comparably expressed in both CD90^{neg/lo} GCTfh and CD90^{hi} GCTfh-like cells (Figure 7A). We also identified a number of genes (*Ccl4*, *Ccr4*, *Ccr10*, *E2f1*, *E2f7*, *E2f8*, *Il2*, and *Sema4a*) that were significantly upregulated in CD90^{hi} GCTfh-like cells compared with CD90^{neg/lo} GCTfh cohorts (Figures 7B–7E). These genes are not known to be Tfh-related but are associated with T cell activation, proliferation, and migration (Attwooll et al., 2004; Lu et al., 2018; Stein and Nombela-Arrieta, 2005).

To infer functional differences from the distinctive transcriptomes of the CD90^{neg/lo} GCTfh and CD90^{hi} GCTfh-like populations, we performed gene set enrichment analysis (GSEA) against the gene ontology database (C5; MSigDB) to identify ontological pathways associated with the gene expression patterns of these two populations. Significant gene sets (FDR < 0.1 or $p < 0.01$) were visualized as interaction networks with Cytoscape and Enrichment Map (Figures 7F and S7E; Table S1) (Merico et al., 2010). Compared with CD90^{hi} GCTfh-like cells, the CD90^{neg/lo} GCTfh subset was significantly enriched for gene expression profiles linked to endosome/vesicle organization and exocytosis/degranulation (Figures 7F and S7E; Table S1). Expression of genes associated with vesicle organization and/or exocytosis (*Apoe*, *Enpp1*, *Gapapar11*, *Gem*, *Itmb2b*,

Lamp1, *Lyn*, *Map1lc3b*, *Optn*, *P2rx4*, *Pfn2*, *Pla2g7*, *Rnf128*, *Sdc4*, *Sh3gl3*, *Sh3tc1*, *Sytl3*, *Tmem9*, and *Zfyve28*) was significantly elevated in CD90^{neg/lo} GCTfh cells (Figure 7G), whereas genes downregulated during vesicle organization and/or exocytosis (*Anxa5*, *Anxa6*, *Kremen2*, *Ldlr*, *Rab3d*, and *Sor1*) were suppressed (Figure 7G). Notably, gene expression indicative of activated lipid and steroid metabolism (Table S1) was also significantly enriched in CD90^{neg/lo} GCTfh cells.

CD90^{hi} GCTfh-like cells showed patterns of gene expression associated with cell division (Figures 7F and S7E–S7F; Table S1), consistent with the more abundant numbers of Ki-67⁺ cells in this compartment (Figures 3A and 3C). CD90^{hi} GCTfh-like cells also expressed genes related to cell migration and chemotaxis (*Ccl3*, *Ccl4*, *Ccr4*, *Ccr5*, *Ccr6*, *Ccr7*, *Ccr10*, *Cxcl13*, *Cxcr3*, *Dock4*, *Gpr18*, *Gpr183*, *Hmgb2*, *Selplg*, *Sell*, and *Tbx21*) (Moriyama et al., 2014) (Figure S7G) and protein kinase phosphorylation (*Acvr1l*, *Aurka*, *Aurkb*, *Bub1*, *Bub1b*, *Ccnb1*, *Ccnb2*, *Cdk1*, *Chek1*, *Cit*, *Clspn*, *Gsg2*, *Mastl*, *Melk*, *Nek2*, *Nek6*, *Pbk*, *Plk1*, *Thy1*, and *Ttk*) (Bolanos-Garcia and Blundell, 2011; den Hollander et al., 2010; Gong and Ferrell, 2010; O'Regan et al., 2007) (Figure S7H). Genes generally downregulated during protein kinase phosphorylation, including *Dapk2*, *Lyn*, *Matk*, *Nrbp2*, *Pnck*, and *Spock2*, were suppressed in CD90^{hi} GCTfh-like cells (Figure S7H). In addition, gene expression indicative of activated tissue development and amino acid metabolism was also significantly enriched in CD90^{hi} GCTfh-like cells (Figures 7F and S7E; Table S1). These results indicate distinctive physiologies for CD90^{neg/lo} GCTfh and CD90^{hi} GCTfh-like cells, which were previously obscured by the cellular diversity in the Bcl6⁺ CXCR5^{hi}PD-1^{hi} Tfh population.

DISCUSSION

High-affinity antibody and humoral memory arise in GCs elicited by immunization or infection. In GCs, specialized GCTfh cells appear to act as principal regulators of affinity maturation by selecting higher-affinity GCB cells in the LZ to return to the DZ for additional rounds of mutation and proliferation (Allen et al., 2007; Gitlin et al., 2014). GCTfh cells also direct the output of plasma-cell and memory B cell progeny (Foy et al., 1994; Han et al., 1995; Ise et al., 2018; Randall et al., 1998; Takahashi et al., 1998). Understanding how GCTfh cells guide these humoral reactions is critical to understanding the strength, breadth, and persistence of antibody responses.

We showed by photoactivation and S1pr2-driven labeling that in primary responses, GC-resident Tfh cells are a small subset of the CD4⁺FoxP3⁻Bcl6⁺CXCR5^{hi}PD-1^{hi} population usually designated “GCTfh”; the subset can be identified by reduced or absent expression of CD90. This observation is not novel (Harriman et al., 1990; Zheng et al., 1996), but has been largely neglected. Using CD90 expression to enrich GC-resident Tfh cells from the

(F) GSEA of RNA-seq data. Significant gene sets with FDR < 0.1 or $p < 0.01$ were visualized with Cytoscape and Enrichment Map. The keyword graph represents the annotated results for clustered gene set comparisons. Purple keywords denote the physiological signature enriched in CD90^{neg/lo} GCTfh cells, and green words represent the physiological signature enriched in CD90^{hi} GCTfh-like cells. A detailed graph and lists of gene set comparison information are shown in Figure S7E and Table S1.

(G) Heatmap graph showing the fold-change in expression of significantly ($p < 0.05$) up- or downregulated genes associated with endosomal vesicle organization and exocytosis/degranulation in CD90^{neg/lo} GCTfh over CD90^{hi} GCTfh-like cells. Numbers indicate the value of \log_2 fold-change in gene expression ($n = 3$ at each time point).

larger nonresident GCTfh-like cell population allowed the demonstration of distinctive physiologies for these T cell subsets, which are otherwise phenotypically similar absent artificial genetic marking systems. Loss of CD90 on resident GCTfh cells was observed for multiple immunogens and in the chronic GCs of PPs. Given that TCR signaling in CD4⁺ cells is impaired in CD90-deficient mice or by CD90-blocking antibody (Beissert et al., 1998; Furlong et al., 2017), decreased CD90 on GCTfh cells may be a mechanism for increasing TCR triggering thresholds, perhaps to avoid exhaustion by repetitive interaction with GCB cells (Good-Jacobson et al., 2010). Alternatively, the CD90^{neg/lo} phenotype may represent a novel or unrecognized specialization.

In primary humoral responses, activated Tfh cells leave the T-B border for follicles at day 3, shortly before antigen-activated B cells do the same (Kerfoot et al., 2011; Kitano et al., 2011). With B cell migration, clusters of B cells can be identified at FDC networks, establishing nascent GCs (Kerfoot et al., 2011). In contrast, Tfh cell emigrants are not confined to these primitive GCs but distributed throughout the follicle (Kerfoot et al., 2011). During this early phase of the response, we observed only CD90^{hi} GCTfh-like cells. Reduction of CD90 was observed only after day 5, coincident with the organization of GC LZs and DZs, suggesting that CD90^{neg/lo} GCTfh cells are a component of GC organization. Although peptide+MHCII (pMHCII) presentation on B cells was necessary for the differentiation of CD90^{neg/lo} GCTfh cells, it was not required for the generation of CD90^{hi} GCTfh-like cells. This dichotomy explains how robust Tfh cell migration into follicles, but not FDC networks, can be driven solely by peptide-pulsed DCs (Xu et al., 2013). Together, these findings imply that commitment to the CD90^{neg/lo} GCTfh-cell fate is not fixed until DC-activated CD90^{hi} GCTfh-like cells interact with antigen-presenting B cells and perhaps GCB cells.

The origin of CD90^{neg/lo} GCTfh cells is linked to the CD90^{hi} GCTfh-like cell compartment: some 50% of all Tcrβ rearrangements from CD90^{neg/lo} GCTfh cells are shared with the CD90^{hi} GCTfh-like population. This sharing was stable over time, but the reverse was not: Tcrβ rearrangements from CD90^{hi} GCTfh-like cells diverged from those of the CD90^{neg/lo} GCTfh subset as the response progressed. The most likely explanation for this asymmetric divergence is that as GC responses progress past day 5, input into the non-dividing CD90^{neg/lo} GCTfh subset ends, whereas recruitment, activation, and differentiation of CD90^{hi} GCTfh-like cells persist. We surmise that early in the response, when antigen is abundant, DC-activated pre-Tfh cells become CD90^{hi} GCTfh-like cells and, in turn, may become CD90^{neg/lo} GCTfh cells on cognate interaction with antigen-presenting B cells. Later, when most antigen is retained by DCs and FDCs (Baumjohann et al., 2013; Heesters et al., 2013), pre-Tfh cells can still be activated by DCs but have little chance of encountering activated B cells at the T:B border; consequently, their differentiation is limited to CD90^{hi} GCTfh-like cells. Successful GCTfh-cell development requires the antigen-specific T cell clone to experience serial activation and selection from both DCs and B cells. In the event that pMHCII complexes of DC and B cells differ, the divergence of TCR repertoires in the CD90^{neg/lo} GCTfh and CD90^{hi} GCTfh-like cell compartments might represent selection.

The concept of differing selection by distinct antigen-presenting cell types is consistent with our finding that neither OT-II nor DO11.10 T cells efficiently differentiated into CD90^{neg/lo} GCTfh cells but were highly competent to generate eff non-Tfh and GCTfh-like cells in the presence of endogenous T cell competitors. Both DO11.10 (Murphy et al., 1990) and OT-II (Barnden et al., 1998) transgenic mouse lines express TCRs recovered from T cell hybridomas generated from CD4⁺ T cells selected for continued proliferation *in vitro* in response to irradiated, Ova-pulsed splenocytes (Barnden et al., 1998; White et al., 1983). Given that splenic B cells' ability to present antigen and co-stimulatory signals is radiosensitive, it is likely that selection of Ova-specific blasts was driven by myeloid-derived antigen-presenting cells (Ashwell et al., 1988). We infer that the conditions were not optimal for selecting T cell clones with high potential for GCTfh cell differentiation.

GCTfh cells provide survival and proliferation signals to promote proliferative expansion by higher-affinity GCB cells (Gitlin et al., 2014; Schwickert et al., 2011). This task does not require—and might even be impaired by—GCTfh cell proliferation (Crotty, 2014). Additionally, limiting GCTfh cell numbers may help prevent the dysregulated GC expansion observed in autoimmunity (Vinuesa et al., 2009); indeed, whereas Tfh cells can produce IL-2, they are resistant to IL-2-driven proliferation (Ballesteros-Tato et al., 2012; DiToro et al., 2018). A recent study, however, showed that CXCR5^{hi}PD-1^{hi} Tfh cells continuously divide during the GC reaction (Merkenschlager et al., 2021). Our work now demonstrates that the proliferative CXCR5^{hi}PD-1^{hi} Tfh cells do not include CD90^{neg/lo} GC-resident Tfh cells but rather the CD90^{hi} GCTfh-like cell compartment that carries a transcriptomic signature of persistent cell activation. These CD90^{hi} GCTfh-like cells are generated in the absence of B cell antigen presentation but presumably interact with DCs (Baumjohann et al., 2011; Merkenschlager et al., 2021). Another study reported a quiescent Bcl6-Low Tfh population during GC responses that has some similarities to CD90^{neg/lo} GCTfh cells (Kitano et al., 2011). However, unlike the Bcl6-Low Tfh cells, CD90^{neg/lo} GC-resident Tfh cells did not upregulate *Klf2*, *Il7r*, *Ccr7*, or *S1pr1* transcripts; in fact, CD90^{neg/lo} GCTfh cells downregulated *Klf2*, *Ccr7*, *S1pr1*, and other migration-related genes.

Using CD90 expression to enrich GCTfh from GCTfh-like cells, we demonstrated distinctive physiologies between these phenotypically similar T cell subsets. The population generally described as “GCTfh” cells is, in fact, a composite of subpopulations with dramatic transcriptomic differences, with only a minority representing true GC-resident Tfh cells. Prior studies of GCTfh cells using the Bcl6⁺CXCR5^{hi}PD-1^{hi} phenotype would have encompassed both the dominant GCTfh-like and the less abundant CD90^{neg/lo} GCTfh cells. Indeed, the GCTfh-cell gene signature identified by some of those studies (Choi et al., 2015; Liu et al., 2014; Wing et al., 2017) was readily evident in CD90^{neg/lo} GCTfh cells but less so in GCTfh-like cells; this disparity increased over time as the GC response proceeded from d8 to d24. This observation agrees with previous findings that genes essential for Tfh cell function are expressed most abundantly in S1pr2^{hi} GCTfh cells (Moriyama et al., 2014). Some Tfh-related genes were comparably expressed by CD90^{neg/lo} GCTfh and CD90^{hi} GCTfh-like cells, e.g., *Batf*, *Btla*, *Cd40lg*, *Cxcr5*, *Il4*, *Il6ra*, *Il21*, *Maf*, and *Sh2d1a* (Choi et al.,

2015; Wing et al., 2017). These are presumably important for initial Tfh cell development or common functions in B cell follicles. Finally, the expression of genes related to cell migration and chemotaxis was significantly lower in CD90^{neg/lo} GCTfh cells than in CD90^{hi} GCTfh-like cells, a finding also noted in comparisons of S1pr2^{hi} and S1pr2^{low} Tfh cells (Moriyama et al., 2014); this difference likely reflects their anatomical segregation in and outside of GCs.

Cytokine production by GCTfh cells is limited (Dan et al., 2016), perhaps to focus helper activity to individual GCB cells to avoid bystander activity (Dan et al., 2016; Wan et al., 2019). Indeed, the essential functions of GCTfh are thought to be the repeated expression of membrane CD154 and delivery of neurotransmitters across the T:B cell synapse (Papa et al., 2017; Wan et al., 2019). These findings fit nicely with our RNA-seq data showing that CD90^{neg/lo} GCTfh cells are specialized for endosomal/vesicle organization and exocytosis/degranulation. Because cognate GCTfh cell interactions with GCB cells are brief, lasting ≤ 5 min on average (Shulman et al., 2014), a transcriptome enriched for exocytosis and vesicle transport is consistent with CD90^{neg/lo} GCTfh cells' being capable of efficient and individualized help to GCB cells via immune synapses (Papa and Vinuesa, 2018). Interestingly, transfer of CD154 across the immunological synapse by vesicles to antigen-presenting B cells occurs *in vitro* (Gardell and Parker, 2017), raising the possibility of T cell-help “to go” for GCB cells (Dustin, 2017). That CD90^{neg/lo} GCTfh cells are enriched for vesicle organization and exocytosis pathways is consistent with synapse-dependent help and provides *in vivo* evidence to support the “help to-go” hypothesis (Dustin, 2017). The fact that GCTfh cells can transfer microRNA to GCB cells via extracellular vesicles at synapse formation also supports the potential role of GCTfh cell exosomes in GC development and antibody production (Fernández-Messina et al., 2020).

GC-resident CD90^{neg/lo} GCTfh cells are spatially, functionally, and physiologically distinct from CD90^{hi} GCTfh-like cells, despite sharing the Bcl6⁺CXCR5^{hi}PD-1^{hi} phenotype. Whereas these two subsets appear to share a common origin, the later Tcrβ repertoire differences imply a distinct program of clonal activation and selection for these cohorts, perhaps as a consequence of fate determination driven by cognate interaction with B cells. Regardless of the exact mechanisms that drive this differentiation, identification of CD90^{neg/lo} GCTfh cells has revealed a previously obscured transcriptional program for GC-resident Tfh cells that implies the delivery of individualized help to GCB cells by vesicle exocytosis. Furthermore, the role of residual CD90^{hi} GCTfh-like cells outside the GCs is unclear. Additional investigation of these different Tfh cell subsets will likely provide novel insights into how T and B cells collaborate during humoral responses to protein antigens.

Limitations

Our study focuses only on murine Tfh cells participating in primary or chronic GC responses. By histology, all GC-resident Tfh cells downregulate CD90 but only 40% become RFP⁺ by S1pr2-driven Cre activity. With flow cytometry, all RFP⁺ Tfh cells reduced CD90 expression, as did an equivalent population of RFP⁻ Tfh; we assume these CD90^{neg/lo} RFP⁻ Tfh cells represent the RFP⁻ Tfh cells observed histologically in the GC LZ. We cannot exclude the possibility of S1pr2-independent CD90^{neg/lo} GC-resident Tfh cells. The Zbtb46-DTR model is useful for only

short periods (≤ 8 days) of DC depletion; this limits the window for determining the role of cDCs in GCTfh and GCTfh-like cell differentiation.

STAR★METHODS

Detailed methods are provided in the online version of this paper and include the following:

- KEY RESOURCES TABLE
- RESOURCE AVAILABILITY
 - Lead contact
 - Materials availability
 - Data and code availability
- EXPERIMENTAL MODEL AND SUBJECT DETAILS
 - Mice and immunizations
- METHOD DETAILS
 - Antibodies and flow cytometry
 - Multiphoton imaging and photoactivation
 - Adoptive B cell transfer and mixed bone marrow chimeric mice
 - Adoptive T cell transfer
 - Immunofluorescence staining and microscope
 - DNA extraction and deep sequencing for Tcrβ repertoire analysis
 - RNA extraction, library preparation and sequencing
 - RNA Sequencing data analysis
- QUANTIFICATION AND STATISTICAL ANALYSIS

SUPPLEMENTAL INFORMATION

Supplemental information can be found online at <https://doi.org/10.1016/j.imuni.2021.12.015>.

ACKNOWLEDGMENTS

We thank J. Garnett, D. Liao, X. Nie, A. Watanabe, X. Liang, W. Zhang, and R. Qi for technical assistance. We thank Drs. M. Kuraoka, S. Song, and R. Kotaki for helpful discussion and feedback on the manuscript. We thank Drs. R. Ji and C. Jiang for advice and vibratome use. We thank Dr. E.A. Moseman for advice on multi-photon microscopy. We thank Drs. B. Carlson, Y. Gao, and L. Cameron of the Duke University Light Microscopy Core Facility for imaging equipment and consultation. We thank the Duke University School of Medicine for the use of the Sequencing and Genomic Technologies/Genomic Analysis and Bioinformatics Shared Resource. This work was supported by AI100645, the Duke Center for HIV/AIDS Vaccine Immunology-Immunogen Discovery (CHAVI-ID); AI44371, the Duke Consortium for HIV/AIDS Vaccine Development (CHAVD), Division of AIDS, NIAID, NIH; and by NIH grants AI089618 and AI117892.

AUTHOR CONTRIBUTIONS

C.Y. and G.K. designed the research; C.Y. performed the experiments; T.O. and T.K. provided crucial materials for the study; and C.Y., J.F., and G.K. analyzed data and wrote the manuscript. G.K. directed the study.

DECLARATION OF INTERESTS

The authors declare no competing interests.

Received: October 22, 2020

Revised: September 10, 2021

Accepted: December 21, 2021

Published: January 25, 2022

REFERENCES

- Allen, C.D., Okada, T., Tang, H.L., and Cyster, J.G. (2007). Imaging of germinal center selection events during affinity maturation. *Science* 315, 528–531.
- Ansel, K.M., McHeyzer-Williams, L.J., Ngo, V.N., McHeyzer-Williams, M.G., and Cyster, J.G. (1999). In vivo-activated CD4 T cells upregulate CXC chemokine receptor 5 and reprogram their response to lymphoid chemokines. *J. Exp. Med.* 190, 1123–1134.
- Ashwell, J.D., Jenkins, M.K., and Schwartz, R.H. (1988). Effect of gamma radiation on resting B lymphocytes. II. Functional characterization of the antigen-presentation defect. *J. Immunol.* 141, 2536–2544.
- Attwooll, C., Lazzarini Denchi, E., and Helin, K. (2004). The E2F family: specific functions and overlapping interests. *EMBO J.* 23, 4709–4716.
- Ballesteros-Tato, A., León, B., Graf, B.A., Moquin, A., Adams, P.S., Lund, F.E., and Randall, T.D. (2012). Interleukin-2 inhibits germinal center formation by limiting T follicular helper cell differentiation. *Immunity* 36, 847–856.
- Barnden, M.J., Allison, J., Heath, W.R., and Carbone, F.R. (1998). Defective TCR expression in transgenic mice constructed using cDNA-based alpha- and beta-chain genes under the control of heterologous regulatory elements. *Immunol. Cell Biol.* 76, 34–40.
- Baumjohann, D., Okada, T., and Ansel, K.M. (2011). Cutting Edge: distinct waves of BCL6 expression during T follicular helper cell development. *J. Immunol.* 187, 2089–2092.
- Baumjohann, D., Preite, S., Reboldi, A., Ronchi, F., Ansel, K.M., Lanzavecchia, A., and Sallusto, F. (2013). Persistent antigen and germinal center B cells sustain T follicular helper cell responses and phenotype. *Immunity* 38, 596–605.
- Beissert, S., He, H.T., Hueber, A.O., Lelouch, A.C., Metze, D., Mehling, A., Luger, T.A., Schwarz, T., and Grabe, S. (1998). Impaired cutaneous immune responses in Thy-1-deficient mice. *J. Immunol.* 161, 5296–5302.
- Bolanos-Garcia, V.M., and Blundell, T.L. (2011). BUB1 and BUBR1: multifaceted kinases of the cell cycle. *Trends Biochem. Sci.* 36, 141–150.
- Breitfeld, D., Ohl, L., Kremmer, E., Ellwart, J., Sallusto, F., Lipp, M., and Förster, R. (2000). Follicular B helper T cells express CXC chemokine receptor 5, localize to B cell follicles, and support immunoglobulin production. *J. Exp. Med.* 192, 1545–1552.
- Carlson, C.S., Emerson, R.O., Sherwood, A.M., Desmarais, C., Chung, M.W., Parsons, J.M., Steen, M.S., LaMadrid-Herrmannsfeldt, M.A., Williamson, D.W., Livingston, R.J., et al. (2013). Using synthetic templates to design an unbiased multiplex PCR assay. *Nat. Commun.* 4, 2680.
- Cho, S., Lee, H.M., Yu, I.S., Choi, Y.S., Huang, H.Y., Hashemifar, S.S., Lin, L.L., Chen, M.C., Afanasiev, N.D., Khan, A.A., et al. (2018). Differential cell-intrinsic regulations of germinal center B and T cells by miR-146a and miR-146b. *Nat. Commun.* 9, 2757.
- Choi, Y.S., Gullicksrud, J.A., Xing, S., Zeng, Z., Shan, Q., Li, F., Love, P.E., Peng, W., Xue, H.H., and Crotty, S. (2015). LEF-1 and TCF-1 orchestrate T(FH) differentiation by regulating differentiation circuits upstream of the transcriptional repressor Bcl6. *Nat. Immunol.* 16, 980–990.
- Choi, Y.S., Kageyama, R., Eto, D., Escobar, T.C., Johnston, R.J., Monticelli, L., Lao, C., and Crotty, S. (2011). ICOS receptor instructs T follicular helper cell versus effector cell differentiation via induction of the transcriptional repressor Bcl6. *Immunity* 34, 932–946.
- Choi, Y.S., Yang, J.A., Yusuf, I., Johnston, R.J., Greenbaum, J., Peters, B., and Crotty, S. (2013). Bcl6 expressing follicular helper CD4 T cells are fate committed early and have the capacity to form memory. *J. Immunol.* 190, 4014–4026.
- Cirelli, K.M., Carnathan, D.G., Nogal, B., Martin, J.T., Rodriguez, O.L., Upadhyay, A.A., Enemu, C.A., Gebru, E.H., Choe, Y., Viviano, F., et al. (2019). Slow delivery immunization enhances HIV neutralizing antibody and germinal center responses via modulation of immunodominance. *Cell* 177, 1153–1171.e28.
- Crotty, S. (2011). Follicular helper CD4 T cells (TFH). *Annu. Rev. Immunol.* 29, 621–663.
- Crotty, S. (2014). T follicular helper cell differentiation, function, and roles in disease. *Immunity* 41, 529–542.
- Crotty, S. (2019). T follicular helper cell biology: a decade of discovery and diseases. *Immunity* 50, 1132–1148.
- Dal Porto, Joseph M., Haberman, Ann M., Kelsoe, Garnett, and Shlomchik, Mark J. (2002). Very low affinity B cells form germinal centers, become memory B cells, and participate in secondary immune responses when higher affinity competition is reduced. *Journal of Experimental Medicine* 195, 1215–1221. <https://doi.org/10.1084/jem.20011550>.
- Dal Porto, J.M., Haberman, A.M., Shlomchik, M.J., and Kelsoe, G. (1998). Antigen drives very low affinity B cells to become plasmacytes and enter germinal centers. *J. Immunol.* 161, 5373–5381.
- Dan, J.M., Havenar-Daughton, C., Kendric, K., Al-Kolla, R., Kaushik, K., Rosales, S.L., Anderson, E.L., LaRock, C.N., Vijayanand, P., Seumois, G., et al. (2019). Recurrent group A Streptococcus tonsillitis is an immunosusceptibility disease involving antibody deficiency and aberrant TFH cells. *Sci. Transl. Med.* 11, eaau3776.
- Dan, J.M., Lindestam Arlehamn, C.S., Weiskopf, D., da Silva Antunes, R., Havenar-Daughton, C., Reiss, S.M., Brigger, M., Bothwell, M., Sette, A., and Crotty, S. (2016). A cytokine-independent approach to identify antigen-specific human germinal center T follicular helper cells and rare antigen-specific CD4+ T cells in blood. *J. Immunol.* 197, 983–993.
- den Hollander, J., Rimpi, S., Doherty, J.R., Rudelius, M., Buck, A., Hoellein, A., Kremer, M., Graf, N., Scheerer, M., Hall, M.A., et al. (2010). Aurora kinases A and B are up-regulated by Myc and are essential for maintenance of the malignant state. *Blood* 116, 1498–1505.
- DiToro, D., Winstead, C.J., Pham, D., Witte, S., Andargachew, R., Singer, J.R., Wilson, C.G., Zindl, C.L., Luther, R.J., Silberger, D.J., et al. (2018). Differential IL-2 expression defines developmental fates of follicular versus nonfollicular helper T cells. *Science* 361, eaao2933.
- Dobin, A., Davis, C.A., Schlesinger, F., Drenkow, J., Zaleski, C., Jha, S., Batut, P., Chaisson, M., and Gingeras, T.R. (2013). STAR: ultrafast universal RNA-seq aligner. *Bioinformatics* 29, 15–21.
- Dustin, M.L. (2017). Help to go: T cells transfer CD40L to antigen-presenting B cells. *Eur. J. Immunol.* 47, 31–34.
- Fernández-Messina, L., Rodríguez-Galán, A., de Yébenes, V.G., Gutiérrez-Vázquez, C., Tenreiro, S., Seabra, M.C., Ramiro, A.R., and Sánchez-Madrid, F. (2020). Transfer of extracellular vesicle-microRNA controls germinal center reaction and antibody production. *EMBO Rep.* 21, e48925.
- Foy, T.M., Laman, J.D., Ledbetter, J.A., Aruffo, A., Claassen, E., and Noelle, R.J. (1994). gp39-CD40 interactions are essential for germinal center formation and the development of B cell memory. *J. Exp. Med.* 180, 157–163.
- Furlong, S., Power Coombs, M.R., and Hoskin, D.W. (2017). Thy-1 stimulation of mouse T cells induces a delayed T cell receptor-like signal that results in Ca²⁺-independent cytotoxicity. *Mol. Med. Rep.* 16, 5683–5692.
- Gardell, J.L., and Parker, D.C. (2017). CD40L is transferred to antigen-presenting B cells during delivery of T-cell help. *Eur. J. Immunol.* 47, 41–50.
- Gitlin, A.D., Shulman, Z., and Nussenzweig, M.C. (2014). Clonal selection in the germinal centre by regulated proliferation and hypermutation. *Nature* 509, 637–640.
- Gong, D., and Ferrell, J.E., Jr. (2010). The roles of cyclin A2, B1, and B2 in early and late mitotic events. *Mol. Biol. Cell* 21, 3149–3161.
- Good-Jacobson, K.L., Szumilas, C.G., Chen, L., Sharpe, A.H., Tomayko, M.M., and Shlomchik, M.J. (2010). PD-1 regulates germinal center B cell survival and the formation and affinity of long-lived plasma cells. *Nat. Immunol.* 11, 535–542.
- Green, J.A., Suzuki, K., Cho, B., Willison, L.D., Palmer, D., Allen, C.D., Schmidt, T.H., Xu, Y., Proia, R.L., Coughlin, S.R., and Cyster, J.G. (2011). The sphingosine 1-phosphate receptor S1P₂ maintains the homeostasis of germinal center B cells and promotes niche confinement. *Nat. Immunol.* 12, 672–680.
- Gulbranson-Judge, A., Casamayor-Palleja, M., and MacLennan, I.C. (1997). Mutually dependent T and B cell responses in germinal centers. *Ann. N. Y. Acad. Sci.* 815, 199–210.

- Han, S., Hathcock, K., Zheng, B., Kepler, T.B., Hodes, R., and Kelsoe, G. (1995). Cellular interaction in germinal centers. Roles of CD40 ligand and B7-2 in established germinal centers. *J. Immunol.* **155**, 556–567.
- Haribhai, D., Lin, W., Relland, L.M., Truong, N., Williams, C.B., and Chatila, T.A. (2007). Regulatory T cells dynamically control the primary immune response to foreign antigen. *J. Immunol.* **178**, 2961–2972.
- Harriman, G.R., Lycke, N.Y., Elwood, L.J., and Strober, W. (1990). T lymphocytes that express CD4 and the alpha beta-T cell receptor but lack Thy-1. Preferential localization in Peyer's patches. *J. Immunol.* **145**, 2406–2414.
- Havenar-Daughton, C., Carnathan, D.G., Boopathi, A.V., Upadhyay, A.A., Murrell, B., Reiss, S.M., Enemuo, C.A., Gebru, E.H., Choe, Y., Dhadvai, P., et al. (2019). Rapid germinal center and antibody responses in non-human primates after a single nanoparticle vaccine immunization. *Cell Rep* **29**, 1756–1766.e1758.
- Havenar-Daughton, C., Carnathan, D.G., Torrents de la Pena, A., Pauthner, M., Briney, B., Reiss, S.M., Wood, J.S., Kaushik, K., van Gils, M.J., Rosales, S.L., et al. (2016). Direct probing of germinal center responses reveals immunological features and bottlenecks for neutralizing antibody responses to HIV env trimer. *Cell Rep.* **17**, 2195–2209.
- Haynes, N.M., Allen, C.D., Lesley, R., Ansel, K.M., Killeen, N., and Cyster, J.G. (2007). Role of CXCR5 and CCR7 in follicular Th cell positioning and appearance of a programmed cell death gene-1high germinal center-associated subpopulation. *J. Immunol.* **179**, 5099–5108.
- Heesters, B.A., Chatterjee, P., Kim, Y.A., Gonzalez, S.F., Kuligowski, M.P., Kirchhausen, T., and Carroll, M.C. (2013). Endocytosis and recycling of immune complexes by follicular dendritic cells enhances B cell antigen binding and activation. *Immunity* **38**, 1164–1175.
- Huber, W., Carey, V.J., Gentleman, R., Anders, S., Carlson, M., Carvalho, B.S., Bravo, H.C., Davis, S., Gatto, L., Girke, T., et al. (2015). Orchestrating high-throughput genomic analysis with Bioconductor. *Nat. Methods* **12**, 115–121.
- Ise, W., Fujii, K., Shiroguchi, K., Ito, A., Kometani, K., Takeda, K., Kawakami, E., Yamashita, K., Suzuki, K., Okada, T., and Kurosaki, T. (2018). T follicular helper cell-germinal center B cell interaction strength regulates entry into plasma cell or recycling germinal center cell fate. *Immunity* **48**, 702–715.e4.
- Johnston, R.J., Poholek, A.C., DiToro, D., Yusuf, I., Eto, D., Barnett, B., Dent, A.L., Craft, J., and Crotty, S. (2009). Bcl6 and Blimp-1 are reciprocal and antagonistic regulators of T follicular helper cell differentiation. *Science* **325**, 1006–1010.
- Kelsoe, G. (1996). The germinal center: a crucible for lymphocyte selection. *Semin. Immunol.* **8**, 179–184.
- Kerfoot, S.M., Yaari, G., Patel, J.R., Johnson, K.L., Gonzalez, D.G., Kleinstein, S.H., and Haberman, A.M. (2011). Germinal center B cell and T follicular helper cell development initiates in the interfollicular zone. *Immunity* **34**, 947–960.
- Kersey, P.J., Staines, D.M., Lawson, D., Kulesha, E., Derwent, P., Humphrey, J.C., Hughes, D.S., Keenan, S., Kerhornou, A., Koscielny, G., et al. (2012). Ensembl genomes: an integrative resource for genome-scale data from non-vertebrate species. *Nucleic Acids Res* **40**, D91–D97.
- Kitano, M., Moriyama, S., Ando, Y., Hikida, M., Mori, Y., Kurosaki, T., and Okada, T. (2011). Bcl6 protein expression shapes pre-germinal center B cell dynamics and follicular helper T cell heterogeneity. *Immunity* **34**, 961–972.
- Kuraoka, M., Liao, D., Yang, K., Allgood, S.D., Levesque, M.C., Kelsoe, G., and Ueda, Y. (2009). Activation-induced cytidine deaminase expression and activity in the absence of germinal centers: insights into hyper-IgM syndrome. *J. Immunol.* **183**, 3237–3248.
- Liu, X., Chen, X., Zhong, B., Wang, A., Wang, X., Chu, F., Nurieva, R.I., Yan, X., Chen, P., van der Flier, L.G., et al. (2014). Transcription factor achaete-scute homologue 2 initiates follicular T-helper-cell development. *Nature* **507**, 513–518.
- Liu, Y.J., Zhang, J., Lane, P.J., Chan, E.Y., and MacLennan, I.C. (1991). Sites of specific B cell activation in primary and secondary responses to T cell-dependent and T cell-independent antigens. *Eur. J. Immunol.* **21**, 2951–2962.
- Love, M.I., Huber, W., and Anders, S. (2014). Moderated estimation of fold change and dispersion for RNA-seq data with DESeq2. *Genome Biol.* **15**, 550.
- Lu, N., Li, Y., Zhang, Z., Xing, J., Sun, Y., Yao, S., and Chen, L. (2018). Human Semaphorin-4A drives Th2 responses by binding to receptor ILT-4. *Nat. Commun.* **9**, 742.
- Martin, M. (2011). Cutadapt removes adapter sequences from high-throughput sequencing reads. *EMBnet J.* **17**, 10–12.
- Meli, A.P., and King, I.L. (2015). Identification of mouse T follicular helper cells by flow cytometry. *Methods Mol. Biol.* **1291**, 3–11.
- Meredith, M.M., Liu, K., Darrasse-Jeze, G., Kamphorst, A.O., Schreiber, H.A., Guermonprez, P., Idoyaga, J., Cheong, C., Yao, K.H., Niec, R.E., and Nussenzweig, M.C. (2012). Expression of the zinc finger transcription factor zDC (Zbtb46, Btbd4) defines the classical dendritic cell lineage. *J. Exp. Med.* **209**, 1153–1165.
- Merico, D., Isserlin, R., Stueker, O., Emili, A., and Bader, G.D. (2010). Enrichment map: a network-based method for gene-set enrichment visualization and interpretation. *PLoS One* **5**, e13984.
- Merkenschlager, J., Finkin, S., Ramos, V., Kraft, J., Cipolla, M., Nowosad, C.R., Hartweger, H., Zhang, W., Olinares, P.D.B., Gazumyan, A., et al. (2021). Dynamic regulation of TFH selection during the germinal centre reaction. *Nature* **597**, 458–463.
- Meyer-Hermann, M.E., Maini, P.K., and Iber, D. (2006). An analysis of B cell selection mechanisms in germinal centers. *Math. Med. Biol.* **23**, 255–277.
- Mootha, V.K., Lindgren, C.M., Eriksson, K.F., Subramanian, A., Sihag, S., Lehar, J., Puigserver, P., Carlsson, E., Ridderstråle, M., Laurila, E., et al. (2003). PGC-1alpha-responsive genes involved in oxidative phosphorylation are coordinately downregulated in human diabetes. *Nat. Genet.* **34**, 267–273.
- Moriyama, S., Takahashi, N., Green, J.A., Hori, S., Kubo, M., Cyster, J.G., and Okada, T. (2014). Sphingosine-1-phosphate receptor 2 is critical for follicular helper T cell retention in germinal centers. *J. Exp. Med.* **211**, 1297–1305.
- Murphy, K.M., Heimberger, A.B., and Loh, D.Y. (1990). Induction by antigen of intrathymic apoptosis of CD4+CD8+TCR δ thymocytes in vivo. *Science* **250**, 1720–1723.
- Nance, J.P., Bélanger, S., Johnston, R.J., Takemori, T., and Crotty, S. (2015). Cutting edge: T follicular helper cell differentiation is defective in the absence of Bcl6 BTB repressor domain function. *J. Immunol.* **194**, 5599–5603.
- Nurieva, R.I., Chung, Y., Martinez, G.J., Yang, X.O., Tanaka, S., Matskewitch, T.D., Wang, Y.H., and Dong, C. (2009). Bcl6 mediates the development of T follicular helper cells. *Science* **325**, 1001–1005.
- O'Regan, L., Blot, J., and Fry, A.M. (2007). Mitotic regulation by NIMA-related kinases. *Cell Div.* **2**, 25.
- Papa, I., Saliba, D., Ponzoni, M., Bustamante, S., Canete, P.F., Gonzalez-Figueras, P., McNamara, H.A., Valvo, S., Grimaldeston, M., Sweet, R.A., et al. (2017). TFH-derived dopamine accelerates productive synapses in germinal centres. *Nature* **547**, 318–323.
- Papa, I., and Vinuesa, C.G. (2018). Synaptic interactions in germinal centers. *Front. Immunol.* **9**, 1858.
- Pepper, M., Pagán, A.J., Igártua, B.Z., Taylor, J.J., and Jenkins, M.K. (2011). Opposing signals from the Bcl6 transcription factor and the interleukin-2 receptor generate T helper 1 central and effector memory cells. *Immunity* **35**, 583–595.
- Randall, T.D., Heath, A.W., Santos-Argumedo, L., Howard, M.C., Weissman, I.L., and Lund, F.E. (1998). Arrest of B lymphocyte terminal differentiation by CD40 signaling: mechanism for lack of antibody-secreting cells in germinal centers. *Immunity* **8**, 733–742.
- Robertson, J.M., Jensen, P.E., and Evavold, B.D. (2000). DO11.10 and OT-II T cells recognize a C-terminal ovalbumin 323–339 epitope. *J. Immunol.* **164**, 4706–4712.
- Schaerli, P., Willimann, K., Lang, A.B., Lipp, M., Loetscher, P., and Moser, B. (2000). CXCR5 expression defines follicular homing T cells with B cell helper function. *J. Exp. Med.* **192**, 1553–1562.
- Schmidt, A.G., Therkelsen, M.D., Stewart, S., Kepler, T.B., Liao, H.X., Moody, M.A., Haynes, B.F., and Harrison, S.C. (2015). Viral receptor-binding site antibodies with diverse germline origins. *Cell* **161**, 1026–1034.
- Schwicket, T.A., Victora, G.D., Fooksman, D.R., Kamphorst, A.O., Mugnier, M.R., Gitlin, A.D., Dustin, M.L., and Nussenzweig, M.C. (2011). A dynamic

- T cell-limited checkpoint regulates affinity-dependent B cell entry into the germinal center. *J. Exp. Med.* 208, 1243–1252.
- Shinnakasu, R., Inoue, T., Kometani, K., Moriyama, S., Adachi, Y., Nakayama, M., Takahashi, Y., Fukuyama, H., Okada, T., and Kurosaki, T. (2016). Regulated selection of germinal-center cells into the memory B cell compartment. *Nat. Immunol.* 17, 861–869.
- Shulman, Z., Gitlin, A.D., Targ, S., Jankovic, M., Pasqual, G., Nussenzweig, M.C., and Victora, G.D. (2013). T follicular helper cell dynamics in germinal centers. *Science* 341, 673–677.
- Shulman, Z., Gitlin, A.D., Weinstein, J.S., Lainéz, B., Esplugues, E., Flavell, R.A., Craft, J.E., and Nussenzweig, M.C. (2014). Dynamic signaling by T follicular helper cells during germinal center B cell selection. *Science* 345, 1058–1062.
- Sonoda, E., Pewzner-Jung, Y., Schwers, S., Taki, S., Jung, S., Eilat, D., and Rajewsky, K. (1997). B cell development under the condition of allelic inclusion. *Immunity* 6, 225–233.
- Stein, J.V., and Nombela-Arrieta, C. (2005). Chemokine control of lymphocyte trafficking: a general overview. *Immunology* 116, 1–12.
- Suan, D., Nguyen, A., Moran, I., Bourne, K., Hermes, J.R., Arshi, M., Hampton, H.R., Tomura, M., Miwa, Y., Kelleher, A.D., et al. (2015). T follicular helper cells have distinct modes of migration and molecular signatures in naïve and memory immune responses. *Immunity* 42, 704–718.
- Takahashi, Y., Dutta, P.R., Cerasoli, D.M., and Kelsoe, G. (1998). In situ studies of the primary immune response to (4-hydroxy-3-nitrophenyl)acetyl. V. Affinity maturation develops in two stages of clonal selection. *J. Exp. Med.* 187, 885–895.
- Tubo, N.J., Pagán, A.J., Taylor, J.J., Nelson, R.W., Linehan, J.L., Ertelet, J.M., Huseby, E.S., Way, S.S., and Jenkins, M.K. (2013). Single naïve CD4+ T cells from a diverse repertoire produce different effector cell types during infection. *Cell* 153, 785–796.
- Victora, G.D., Schwickert, T.A., Fooksman, D.R., Kamphorst, A.O., Meyer-Hermann, M., Dustin, M.L., and Nussenzweig, M.C. (2010). Germinal center dynamics revealed by multiphoton microscopy with a photoactivatable fluorescent reporter. *Cell* 143, 592–605.
- Vinuesa, C.G., Sanz, I., and Cook, M.C. (2009). Dysregulation of germinal centres in autoimmune disease. *Nat. Rev. Immunol.* 9, 845–857.
- Wan, Z., Lin, Y., Zhao, Y., and Qi, H. (2019). TFH cells in bystander and cognate interactions with B cells. *Immunol. Rev.* 288, 28–36.
- Wang, P., Shih, C.M., Qi, H., and Lan, Y.H. (2016). A stochastic model of the germinal center integrating local antigen competition, individualistic T-B interactions, and B cell receptor signaling. *J. Immunol.* 197, 1169–1182.
- White, J., Haskins, K.M., Marrack, P., and Kappler, J. (1983). Use of I region-restricted, antigen-specific T cell hybridomas to produce idiotypically specific anti-receptor antibodies. *J. Immunol.* 130, 1033–1037.
- Wing, J.B., Kitagawa, Y., Locci, M., Hume, H., Tay, C., Morita, T., Kidani, Y., Matsuda, K., Inoue, T., Kurosaki, T., et al. (2017). A distinct subpopulation of CD25(-) T-follicular regulatory cells localizes in the germinal centers. *Proc. Natl. Acad. Sci. USA* 114, E6400–E6409.
- Wittenbrink, N., Klein, A., Weiser, A.A., Schuchhardt, J., and Or-Guil, M. (2011). Is there a typical germinal center? A large-scale immunohistological study on the cellular composition of germinal centers during the hapten-carrier-driven primary immune response in mice. *J. Immunol.* 187, 6185–6196.
- Wollenberg, I., Agua-Doce, A., Hernández, A., Almeida, C., Oliveira, V.G., Faro, J., and Graca, L. (2011). Regulation of the germinal center reaction by Foxp3+ follicular regulatory T cells. *J. Immunol.* 187, 4553–4560.
- Wu, H., Xu, L.L., Teuscher, P., Liu, H., Kaplan, M.H., and Dent, A.L. (2015). An inhibitory role for the transcription factor Stat3 in controlling IL-4 and Bcl6 expression in follicular helper T cells. *J. Immunol.* 195, 2080–2089.
- Xu, H., Li, X., Liu, D., Li, J., Zhang, X., Chen, X., Hou, S., Peng, L., Xu, C., Liu, W., et al. (2013). Follicular T-helper cell recruitment governed by bystander B cells and ICOS-driven motility. *Nature* 496, 523–527.
- Yeh, C.H., Nojima, T., Kuraoka, M., and Kelsoe, G. (2018). Germinal center entry not selection of B cells is controlled by peptide-MHCII complex density. *Nat. Commun.* 9, 928.
- Yu, D., Rao, S., Tsai, L.M., Lee, S.K., He, Y., Sutcliffe, E.L., Srivastava, M., Linterman, M., Zheng, L., Simpson, N., et al. (2009). The transcriptional repressor Bcl-6 directs T follicular helper cell lineage commitment. *Immunity* 31, 457–468.
- Yusuf, I., Kageyama, R., Monticelli, L., Johnston, R.J., Ditoro, D., Hansen, K., Barnett, B., and Crotty, S. (2010). Germinal center T follicular helper cell IL-4 production is dependent on signaling lymphocytic activation molecule receptor (CD150). *J. Immunol.* 185, 190–202.
- Zheng, B., Han, S., and Kelsoe, G. (1996). T helper cells in murine germinal centers are antigen-specific emigrants that downregulate Thy-1. *J. Exp. Med.* 184, 1083–1091.

STAR★METHODS

KEY RESOURCES TABLE

REAGENT or RESOURCE	SOURCE	IDENTIFIER
Antibodies		
anti-mouse CD3 AF488 (Clone 17A2)	BioLegend	Cat#100210; RRID: AB_389301
anti-mouse CD3 AF647 (Clone 145-2C11)	BioLegend	Cat#100324; RRID: AB_492861
anti-mouse CD4 Biotin (Clone GK1.5)	BioLegend	Cat#100404; RRID: AB_312689
anti-mouse CD4 AF647 (Clone GK1.5)	BioLegend	Cat#100424; RRID: AB_389324
anti-mouse CD4 AF647 (Clone RM4-5)	BioLegend	Cat#100533; RRID: AB_493372
anti-mouse CD4 BV421 (Clone GK1.5)	BioLegend	Cat#100443; RRID: AB_2562557
anti-mouse CD4 BV510 (Clone RM4-5)	BD Biosciences	Cat#563106; RRID: AB_2687550
anti-mouse CD8 BV421 (Clone 53-6.7)	BD Biosciences	Cat#563898; RRID: AB_2738474
anti-mouse CD11b PE-Cy7 (Clone M1/70)	BioLegend	Cat#101215; RRID: AB_312798
anti-mouse CD11c Biotin (Clone N418)	BioLegend	Cat#117304; RRID: AB_313773
anti-mouse CD11c AF647 (Clone N418)	BioLegend	Cat#117312; RRID: AB_389328
anti-mouse CD19 APC-R700 (Clone 1D3)	BD Biosciences	Cat#565473; RRID: AB_2739253
anti-mouse CD21/35 AF594 (Clone 7E9)	BioLegend	Cat#123426; RRID: AB_2632698
anti-mouse CD21/35 AF647 (Clone 7E9)	BioLegend	Cat#123424; RRID: AB_2629578
anti-mouse CD25 BV421 (Clone PC61)	BioLegend	Cat#102043; RRID: AB_2562611
anti-mouse CD43 Biotin (Clone S7)	BD Biosciences	Cat#553269; RRID: AB_2255226
anti-mouse/human CD44 FITC (Clone IM7)	BioLegend	Cat#103006; RRID: AB_312957
anti-mouse/human CD44 PerCP-Cy5.5 (Clone IM7)	BioLegend	Cat#103006; RRID: AB_2076204
anti-mouse/human CD44 PE-594 (Clone IM7)	BioLegend	Cat#103056; RRID: AB_2564044
anti-mouse CD45.1 BV421 (Clone A20)	BioLegend	Cat#110732; RRID: AB_2562563
anti-mouse CD45.2 FITC (Clone 104)	Thermo Fisher Scientific	Cat#11-0454-82; RRID: AB_465061
anti-mouse CD62L PerCP-Cy5.5 (Clone MEL-14)	BioLegend	Cat#104430; RRID: AB_2187124
anti-mouse CD62L PE (Clone MEL-14)	BioLegend	Cat#104408; RRID: AB_313095
anti-mouse CD62L BV786 (Clone MEL-14)	BD Biosciences	Cat#564109; RRID: AB_2738598
anti-mouse CD69 PE-Cy5 (Clone H1.2F3)	BioLegend	Cat#104510; RRID: AB_313113
anti-mouse CD90.2 Biotin (Clone 30H12)	BioLegend	Cat#105304; RRID: AB_313175
anti-mouse CD90.2 AF488 (Clone 30H12)	BioLegend	Cat#105316; RRID: AB_492886
anti-mouse CD90.2 PE (Clone 30H12)	BioLegend	Cat#105307; RRID: AB_313178
anti-mouse CD90.2 AF647 (Clone 30H12)	BioLegend	Cat#105318; RRID: AB_492888
anti-mouse CD90.2 AF700 (Clone 30H12)	BioLegend	Cat#105320; RRID: AB_493725
anti-mouse CD90.2 AF700 (Clone 53-2.1)	BioLegend	Cat#140324; RRID: AB_2566740
anti-mouse CD90.2 BV421 (Clone 53-2.1)	BioLegend	Cat#140327; RRID: AB_2686992
anti-mouse CD138 BV308 (Clone 281-2)	BD Biosciences	Cat#563147; RRID: AB_2721029
anti-mouse CD185 (CXCR5) Biotin (Clone L138D7)	BioLegend	Cat#145510; RRID: AB_2562126
anti-mouse CD185 (CXCR5) Biotin (Clone 2G8)	BD Biosciences	Cat#551960; RRID: AB_394301
anti-mouse CD279 (PD-1) PE-Cy7 (Clone 29F.1A12)	BioLegend	Cat#135216; RRID: AB_10689635
anti-mouse CD279 (PD-1) BV421 (Clone 29F.1A12)	BioLegend	Cat#135221; RRID: AB_2562568
anti-mouse/human B220 APC/Fire750 (Clone RA3-6B2)	BioLegend	Cat#103259; RRID: AB_2572108

(Continued on next page)

Continued

REAGENT or RESOURCE	SOURCE	IDENTIFIER
anti-mouse/human B220 BV605 (Clone RA3-6B2)	BioLegend	Cat#103244; RRID: AB_2563312
anti-mouse/human B220 BV785 (Clone RA3-6B2)	BioLegend	Cat#103246; RRID: AB_2563256
anti-mouse/human Bcl-6 PE (Clone K112-91)	BD Biosciences	Cat#561522; RRID: AB_10717126
anti-mouse/human Bcl-6 PE-CF594 (Clone K112-91)	BD Biosciences	Cat#562401; RRID: AB_11152084
anti-mouse/human Bcl-6 AF647 (Clone K112-91)	BD Biosciences	Cat#561525; RRID: AB_10898007
anti-mouse DO11.10 TCR FITC (Clone KJ1-26)	Thermo Fisher Scientific	Cat#11-5808-82; RRID: AB_465248
anti-mouse F4/80 Biotin (Clone BM8)	BioLegend	Cat#123106; RRID: AB_893501
anti-mouse F4/80 PE (Clone BM8)	BioLegend	Cat#123110; RRID: AB_893486
anti-mouse FoxP3 AF488 (Clone FJK-16s)	Thermo Fisher Scientific	Cat#53-5773-82; RRID: AB_763537
anti-mouse FoxP3 AF647 (Clone MF23)	BD Biosciences	Cat#560401; RRID: AB_1645201
anti-GFP AF488 (Clone FM264G)	BioLegend	Cat#338008; RRID: AB_2563288
anti-mouse GL7 FITC (Clone GL7)	BD Biosciences	Cat#553666; RRID: AB_394981
anti-mouse GL7 PE (Clone GL7)	BD Biosciences	Cat#561530; RRID: AB_10715834
anti-mouse Gr-1 PE (Clone RB6-8C5)	BioLegend	Cat#108404; RRID: AB_313369
anti-human HB-EGF (Goat Polyclonal)	R&D Systems	Cat#BAF259; RRID: AB_2114598
anti-mouse I-A/I-E (MHCII) AF647 (Clone M5/114.15.2)	BioLegend	Cat#107618; RRID: AB_493525
anti-mouse I-A/I-E (MHCII) BV711 (Clone M5/114.15.2)	BD Biosciences	Cat#563414; RRID: AB_2738191
anti-mouse I-Ab (MHCII) PE-CF594 (Clone AF6-120.1)	BD Biosciences	Cat#562824; RRID: AB_2737819
anti-mouse IgD BV421 (Clone 11-26c.2a)	BioLegend	Cat#405725; RRID: AB_2562743
anti-mouse IgD BV510 (Clone 11-26c.2a)	BioLegend	Cat#405723; RRID: AB_2562742
anti-mouse Ig κ light chain BV421 (Clone 187.1)	BD Biosciences	Cat#562888; RRID: AB_2737867
anti-mouse Ig λ1, λ2, & λ3 light chain FITC (Clone R26-46)	BD Biosciences	Cat#553434; RRID: AB_394854
anti-mouse/human Ki-67 BV421 (Clone 11F6)	BioLegend	Cat#151208; RRID: AB_2629748
anti-mouse/human Ki-67 BV421 (Clone B56)	BD Biosciences	Cat#562899; RRID: AB_2686897
anti-mouse/human Ki-67 AF647 (Clone B56)	BD Biosciences	Cat#558615; RRID: AB_647130
anti-mouse/human Ki-67 BV650 (Clone B56)	BD Biosciences	Cat#563757; RRID: AB_2688008
anti-mouse Ly6C FITC (Clone AL21)	BD Biosciences	Cat#553104; RRID: AB_394628
anti-RFP (Rabbit Polyclonal)	Rockland	Cat#600-401-379; RRID: AB_2209751
anti-mouse TCRβ FITC (Clone H57-597)	BioLegend	Cat#109205; RRID: AB_313428
anti-mouse TCRβ PE-Cy7 (Clone H57-597)	BioLegend	Cat#109221; RRID: AB_893627
anti-mouse TCRβ BV711 (Clone H57-597)	BD Biosciences	Cat#563135; RRID: AB_2738023
anti-mouse TCR Vβ5.1/5.2 PE (Clone MR9-4)	BD Biosciences	Cat#562086; RRID: AB_394698
anti-mouse Ter-119 Biotin (Clone TER-119)	BioLegend	Cat#116204; RRID: AB_313705
anti-Rabbit IgG (H+L) AF594 (Goat Polyclonal)	Thermo Fisher Scientific	Cat#A-11012; RRID: AB_2534079

(Continued on next page)

Continued

REAGENT or RESOURCE	SOURCE	IDENTIFIER
anti-mouse CD16/CD32 (Mouse BD Fc Block™)	BD Biosciences	Cat#553142; RRID: AB_394656
Chemicals, peptides, and recombinant proteins		
Acetone	Sigma-Aldrich	Cat#179124
Alhydrogel® adjuvant 2%	InvivoGen	Cat#vac-alu-250
Corn oil	Sigma-Aldrich	Cat#PHR2897
Diphtheria Toxin from <i>Corynebacterium diphtheriae</i>	Sigma-Aldrich	Cat#D0564
IgG from rat serum	Sigma-Aldrich	Cat#I4131
Methanol	Sigma-Aldrich	Cat#34860
NP ₁₀ -HSA (Human Serum Albumin)	Biosearch Technologies	Cat#N-5059-10
NP ₁₅ -Ova (Ovalbumin)	Biosearch Technologies	Cat#N-5051-100
Ovalbumin	Biosearch Technologies	Cat#O-1000-100
recombinant PA (Protective antigen)	BEI Resources	NR-36208
recombinant HA (A/Solomon Islands/3/2006)	S. Harrison	(Schmidt et al., 2015)
16% Formaldehyde (w/v), Methanol-free	Thermo Fisher Scientific	Cat#28906
Streptavidin AF488	BioLegend	Cat#405235
Streptavidin PE	BioLegend	Cat#405204
Streptavidin APC	BioLegend	Cat#405207
Streptavidin BV421	BioLegend	Cat#405225
Streptavidin BV650	BioLegend	Cat#405232
Sucrose	Sigma-Aldrich	Cat#S9378
Tamoxifen	Sigma-Aldrich	Cat#T5648
Tissue-Tek® O.C.T. Compound	Sakura Finetek USA	Cat#4583
Critical commercial assays		
Direct-zol RNA Miniprep	Zymo Research	Cat#R2051
immunoSEQ mouse Tcrβ assay	Adaptive Biotechnologies	https://www.immunoseq.com/assays/
KAPA HyperPlus Kit	Roche Molecular Systems	Cat#07962401001
KAPA Pure Beads	Roche Molecular Systems	Cat#07983280001
LIVE/DEAD™ Fixable Near-IR Dead Cell Stain Kit	Thermo Fisher Scientific	Cat#L34976
Pan T Cell Isolation Kit II	Miltenyi Biotec	Cat#130-095-130
Qubit dsDNA HS Assay Kit	Thermo Fisher Scientific	Cat#Q32851
Qubit RNA IQ Assay	Thermo Fisher Scientific	Cat#Q33222
RNA 6000 Pico kit	Agilent	Cat#5067-1513
SMART-Seq® v4 Ultra Low Input RNA Kit	Takara Bio	Cat#634890
Streptavidin MicroBeads	Miltenyi Biotec	Cat#130-048-101
Transcription Factor Buffer Set	BD Biosciences	Cat#562574
Deposited data		
RNA-seq data	This paper	GEO: GSE147035
Tcrβ sequence data	This paper	https://clients.adaptivebiotech.com/pub/yeh-2021-immunity DOI: https://dx.doi.org/10.21417/cy2021
Experimental models: Organisms/strains		
Mouse: C57BL/6J (B6)	The Jackson Laboratory	JAX: 000664
Mouse: B6.129S2-H2 ^{d1Ab1-Ea} /J (MHCII ^{−/−})	The Jackson Laboratory	JAX: 003584
Mouse: B6.SJL-Ptprc ^a Pepc ^b /BoyJ (B6.CD45.1)	The Jackson Laboratory	JAX: 002014

(Continued on next page)

Continued

REAGENT or RESOURCE	SOURCE	IDENTIFIER
Mouse: B6.Cg-Ptprc ^a Tg(UBC-PA-GFP) 1Mnz/J (PAGFP)	The Jackson Laboratory	JAX: 022486
Mouse: B6.Cg-Foxp3 ^{tm2Tch} /J (FoxP3 ^{EGFP})	The Jackson Laboratory	JAX: 006772
Mouse: B6(Cg)-Zbtb46 ^{tm1(HBEGF)Mnz} /J (zbtb46-DTR)	The Jackson Laboratory	JAX: 019506
Mouse: B6.129S2-Ighm ^{tm1Cgn} /J (μ MT)	The Jackson Laboratory	JAX: 002288
Mouse: B6.C(Cg)-Cd79a ^{tm1(cre)Reth} /EhobJ (Mb1 ^{Cre})	The Jackson Laboratory	JAX: 020505
Mouse: B6.Cg-Tg(TcraTcrb)425Cbn/J (OT-II Tg)	The Jackson Laboratory	JAX: 004194
Mouse: C57BL/6-Gt(ROSA)26Sor ^{tm1(HBEGF)Awai} /J (DTR ^{LSL})	The Jackson Laboratory	JAX: 007900
Mouse: B6.Cg-Gt(ROSA)26Sor ^{tm14(CAG-tdTomato)Hze} /J	The Jackson Laboratory	JAX: 007914
Mouse: Balb/cJ (Balb/c)	The Jackson Laboratory	JAX: 000651
Mouse: C.Cg-Tg(DO11.10)10Dlo/J (DO11.10 Tg)	The Jackson Laboratory	JAX: 003303
Mouse: CByJ.SJL(B6)-Ptprc ^a /J (Balb/c.CD45.1)	The Jackson Laboratory	JAX: 006584
Mouse: Tg(S1pr2-cre/ERT2)#Kuro (S1pr2 ^{ERT2Cre})	(Shinnakasu et al., 2016)	MGI: 6435090
Mouse: Ig ^{tm2Cgn} (B1-8i)	(Sonoda et al., 1997)	MGI: 2388486
Mouse: B6.H50G μ	((Dal Porto et al., 2002))	PMC2193705
Software and algorithms		
BD FACSDiva Software	BD Biosciences	http://www.bdbiosciences.com/instruments/software/facsdiva/index.jsp RRID:SCR_001456
Bioconductor	Huber et al., 2015	http://www.bioconductor.org/ RRID:SCR_006442
Cytoscape	National Institute of General Medical Sciences	http://cytoscape.org RRID:SCR_003032
DESeq2	Love et al., 2014	https://bioconductor.org/packages/release/bioc/html/DESeq2.html RRID:SCR_015687
EnrichmentMap	Merico et al., 2010	http://baderlab.org/Software/EnrichmentMap RRID:SCR_016052
Fiji (ImageJ)	National Institutes of Health	http://fiji.sc/ RRID: SCR_002285
FlowJo	BD	https://www.flowjo.com/solutions/flowjo RRID:SCR_008520
GraphPad Prism_V9	GraphPad Software	https://www.graphpad.com/scientific-software/prism/ RRID: SCR_002798
HTSeq tool	European Molecular Biology Laboratory	http://www-huber.embl.de/users/anders/HTSeq/ RRID:SCR_004473
immunoSEQ ANALYZER	Adaptive Biotechnologies (Carlson et al., 2013)	https://clients.adaptivebiotech.com/
STAR RNAseq alignment tool	Dobin et al., 2013	http://code.google.com/p/rna-star/ RRID:SCR_016533
Trim Galore toolkit	Martin, 2011	http://www.bioinformatics.babraham.ac.uk/projects/trim_galore RRID:SCR_011847

RESOURCE AVAILABILITY**Lead contact**

Requests for further information, resources, and reagents should be directed to the lead contact, Garnett Kelsoe (garnett.kelsoe@duke.edu).

Materials availability

All materials in this study are available from the lead contact upon reasonable request.

Data and code availability

RNA-seq data have been deposited at GEO and are publicly available as of the date of publication. Accession numbers are listed in the key resources table. All Tcr β sequence data sets are available from Adaptive Biotechnologies immuneACCESS and are publicly available as of the date of publication. Direct links are listed in the key resources table. Any additional information required to reanalyze the data reported in this paper is available from the lead contact upon request.

EXPERIMENTAL MODEL AND SUBJECT DETAILS

Mice and immunizations

B6, B6.CD45.1, MHCII $^{/-}$, PAGFP, FoxP3^{EGFP}, Zbtb46-DTR, μ MT, Mb1^{Cre}, OT-II Tg, DTR^{LSL}, DO11.10 Tg and Balb/c.CD45.1 mice were purchased from the Jackson Laboratory (see [KEY RESOURCES TABLE](#)). S1pr2^{ERT2Cre}-Rosa26^{lox-stop-lox-tdTomato} mice ([Shinnaka et al., 2016](#)) were provided by T. Kurosaki at Osaka University, B1-8i mice ([Sonoda et al., 1997](#)) were provided by K. Rajewsky at MDC Berlin, and B6.H50G μ mice maintained in our laboratory ([Dal Porto et al., 2002](#)). All mice were maintained under specific pathogen-free, temperature- and humidity-controlled conditions at the Duke University Animal Care Facility and used in experiments at 8 to 12 weeks of age. Due to the limited availability of special strains and chimeric mice, no randomization was used. The investigator was not blinded to group allocation during the animal experiments. Sample size to ensure adequate statistical power was based on prior experience in the laboratory. Mice were footpad-immunized with 20 μ g of NP₁₅-Ova, NP₁₀-HSA, Ova, rPA, or rHA (A/Solomon Islands/3/2006) ([Schmidt et al., 2015](#)) in Alhydrogel® adjuvant 2% (1:1, v/v) in a final volume of 20 μ L. Draining pLN samples were collected at indicated time points post-immunization. Deletion of the loxP-flanked STOP cassette in S1pr2^{ERT2Cre}-Rosa26^{lox-stop-lox-tdTomato} mice was induced by i.p. injection of 5 mg tamoxifen in corn oil once daily on day 5-7. Depletion of Mb1^{Cre}xDTR^{LSL} B cells or Zbtb46-DTR cDCs in chimeric mice was induced by i.p. injection of 20 ng/gwt diphtheria toxin in PBS at indicated starting time points, followed by 4 ng/gwt injection every two days. All experimental procedures involving animals were approved by the Duke University Institutional Animal Care and Use Committee.

METHOD DETAILS

Antibodies and flow cytometry

For surface marker detection, cells were suspended in PBS containing 0.5% bovine serum albumin, 0.1% sodium azide and 1 mM EDTA (FACS buffer). Samples were blocked with rat anti-mouse CD16/32 and rat IgG in FACS buffer for 30 minutes and stained with fluorochrome-conjugated antibodies at 4°C for 30-40 minutes (for antibody clones see [KEY RESOURCES TABLE](#)). LIVE/DEAD Fixable Near-IR Dead Cell Stain Kit was used to exclude dead cells. For nuclear or intracellular staining, samples were fixed, permeabilized, and stained using BD Transcription Factor Buffer Set. Subsequently, cells were washed twice with FACS buffer, and the re-suspended cells were then analyzed on LSRII or LSRFortessa cell analyzers (BD Biosciences). Fluorescence-activated cell sorting was performed with a FACSAria sorter (BD Biosciences). Data analysis was performed with FACSDiva and FlowJo software. Cell gating strategies are described in [Figures S1, S3A, S3I and S7A](#). Flow cytometry was performed in the Duke Human Vaccine Institute Flow Cytometry Facility (Durham, NC).

Multiphoton imaging and photoactivation

PAGFP mice were footpad-immunized with 20 μ g of NP-Ova+alum. AF594-conjugated anti-CD21/CD35 antibody (5 μ g) was s.c. injected into the hock 16-24 hours prior to tissue harvest. Draining pLN slices were harvested and immediately embedded in 4% low-melting-point agarose, followed by sectioning into 250 μ m slices with a Leica VT1200S vibratome. LN slices were firmly attached to the bottom of cell culture dish filled with 1x HBSS. All imaging was performed on a Leica SP8 multi-photon DIVEx microscope fitted with a 25X 1.05NA dipping objective and two tunable fSec Ti:Saph lasers (680-1080 nm and 680-1300 nm). Background GFP and FDC networks labeled with AF594-conjugated anti-CD21/CD35 antibody were visualized using $\lambda = 940$ nm and 1100 nm excitation, simultaneously. GC area were photoactivated using $\lambda = 830$ nm light and the photoactivated area was subsequently visualized with $\lambda = 940$ and 1100 nm excitation light. The photoactivated tissue sections were recovered and subjected to flow cytometric analysis.

Adoptive B cell transfer and mixed bone marrow chimeric mice

For short-term cell transfers, single-B-cell suspensions were harvested and processed from spleens of B1-8i or Mb1^{Cre}xDTR^{LSL} mice. Splenocytes were first stained with a mixture of biotinylated-Abs (anti-CD4, anti-CD11c, anti-CD43, anti-CD90.2, anti-F4/80, anti-Gr-1 and anti-Ter119) and subsequently labeled with Streptavidin MicroBeads. B cells were then negatively purified using magnet-activated cell sorting in a CS column on a VarioMACS separator (Miltenyi Biotec). For B1-8i B cells, B cell-enriched samples were stained and sorted using flow cytometry to acquire B220⁺Ig λ ⁺IgD⁺ B1-8i B cells. Single-cell suspension containing indicated numbers of purified B cells in 200 μ L PBS were i.v. transferred to individual recipient mice. To generate mixed BM chimeric mice, C57BL/6 mice were lethally irradiated with two doses of 600 rad X-ray 3 hours apart and then i.v. injected 5 \times 10⁶ mixed BM cells. The BM mixture were made with 80:20 ratio of BM cells harvested from B6 or μ MT and MHCII $^{/-}$ mice. Reconstituted mice were

rested for 8 weeks before use in experiments. To generate zbtb46-DTR chimeric mice, C57BL/6 mice were lethally irradiated with two doses of 600 rad X-ray 3 hours apart and then i.v. injected with 5×10^6 of BM cells harvested from B6 or zbtb46-DTR mice. Reconstituted mice were rested for 8 weeks before use in experiments.

Adoptive T cell transfer

For transgenic T cell transfers, single-cell suspensions were harvested and processed from spleens of CD45.1⁺ OT-II or DO11.10 TCR transgenic mice. Splenocytes were first stained with a mixture of biotinylated-Abs (anti-CD8a, anti-CD11b, anti-CD11c, anti-CD19, anti-CD25, anti-CD45R (B220), anti-CD49b (DX5), anti-CD105, Anti-MHCII, anti-Ter-119, and anti-TCR γ/δ) and subsequently labeled with Streptavidin MicroBeads. CD4⁺ T cells were then negatively purified using magnet-activated cell sorting in a CS column on a VarioMACS separator (Miltenyi Biotec). T cell-enriched samples were stained and analyzed using flow cytometry to determine the purity and percentage of transgenic TCR-bearing populations. Single cell suspensions containing 2×10^6 of CD4⁺ T cells in 200 μL PBS were i.v. transferred to individual recipient CD45.2⁺ B6 or Balb/c mice. Reconstituted mice were rested overnight (16–24 hours) before immunization.

Immunofluorescence staining and microscope

Harvested pLN samples were embedded in Tissue-Tek OCT Compound and frozen at -80°C. Cryosectioning was performed on a Leica CM1850 Cryostat and fixed in cold acetone/methanol (1:1) at -20°C for 10 minutes. For S1pr2-RFP mice, the pLN samples were pre-fixed with 1% PFA overnight, followed by gradient sucrose dehydration. Tissue sections (5–10 μm -thick) were mounted on glass slides and rehydrated by soaking in wash solution (PBS containing 0.5% BSA and 0.1% Tween-20) at RT for 30 minutes. Samples were then blocked with rat anti-mouse CD16/CD32 and rat IgG for 15 min at room temperature. After washing, the samples were incubated with antibodies for CD3 (17A2 or 145-2C11), CD4 (GK1.5 or RM4-5), CD21/CD35 (7E9), CD90.2 (53-2.1 or 30-H12), Bcl6 (K112-91), Ki-67 (11F6), IgD (11-26c.2a) and anti-RFP Ab in a humid, dark chamber for 3 hours at RT or 4°C overnight (see [KEY RESOURCES TABLE](#)). After washing, the samples were then incubated with secondary or enhancing antibodies for 1 hour at RT. Images were acquired by confocal microscopy using a Zeiss LSM 780 confocal microscope. Image processing, including counting cells in GCs, was performed using ImageJ software (Fiji package).

DNA extraction and deep sequencing for Tcr β repertoire analysis

The TCR β repertoire of CD4⁺ T cells was analyzed using the immunoSEQ mouse Tcr β assay (Adaptive Biotechnologies; ([Carlson et al., 2013](#))). FoxP3^{EGFP} mice were footpad-immunized with 20 μg of NP-Ova+alum. pLNs were harvested at indicated time points. CD90^{neg/lo} GCTfh and CD90^{hi} GCTfh-like cells sorted from the same pLN were subjected to genomic DNA extraction using a phenol/chloroform method ([Kuraoka et al., 2009](#)). Isolated genomic DNA was sent to Adaptive Biotechnologies, which performed multiplex PCR amplification of all possible rearranged *Tcrb* genes from gDNA samples and high-throughput deep sequencing using Illumina HiSeq platform. The raw HiSeq sequence data were preprocessed to remove errors and to compress the data. Tcr β sequences were characterized and analyzed with the Adaptive immunoSEQ Analyzer ([Carlson et al., 2013](#)).

RNA extraction, library preparation and sequencing

RNA was extracted from sorted cell populations using a Direct-zol RNA Kit. RNA quality and concentration were determined with a Qubit 4.0 fluorimeter (Thermo Fisher Scientific) with the RNA IQ Assay and a Bioanalyzer (Agilent) with Agilent RNA 6000 Pico Kit. Only samples with RIN > 8 were proceed to reverse transcription. cDNA was synthesized with the SMART-Seq® v4 Ultra Low Input RNA Kit following manufacturer's recommendations. Adapters were used as priming sites for cDNA synthesis and downstream PCR to amplify the cDNA. Amplified cDNA was purified using KAPA Pure Beads, and the yield and quality were determined with a Qubit 4.0 fluorimeter using the dsDNA HS Assay Kit. The DNA library was constructed using a KAPA HyperPlus Kit, following the manufacturer's recommendations. Sequencing was performed using a HiSeq 4000 system (Illumina) at the Duke University Center for Genomic and Computational Biology.

RNA Sequencing data analysis

RNAseq data were processed using the TrimGalore toolkit which employs Cutadapt ([Martin, 2011](#)) to trim low-quality bases and Illumina sequencing adapters from the 3' end of the reads. Only reads that were 20 nucleotides or longer after trimming were retained for further analysis. Reads were mapped to the GRCm38v73 version of the mouse genome and transcriptome ([Kersey et al., 2012](#)) using the STAR RNAseq alignment tool ([Dobin et al., 2013](#)). Reads were retained for subsequent analysis if they mapped to a single genomic location. Gene counts were compiled using the HTSeq tool. Only genes that had at least 10 reads in any given library were used in subsequent analyses. Normalization and differential expression analysis was carried out using the DESeq2 ([Love et al., 2014](#)) Bioconductor ([Huber et al., 2015](#)) package with the R statistical programming environment. The false discovery rate was calculated to control for multiple hypothesis testing. Gene set enrichment analysis was performed to identify gene ontology terms and pathways associated with altered gene expression for each of the comparisons performed ([Mootha et al., 2003](#)). Network visualization of gene set enrichment was performed using Cytoscape Version 3.7.2 and the plugin "Enrichment Map" to build the network and the plugin "AutoAnnotate" to build clusters with visual annotations ([Merico et al., 2010](#)).

QUANTIFICATION AND STATISTICAL ANALYSIS

Statistical analyses were performed using ordinary analysis of variance (ANOVA) followed by Tukey's or Dunnett's post-tests or two-way ANOVA followed by Sidak's post-test. Differences were considered statistically significant at P values < 0.05 (*P<0.05; **P<0.01; ***P<0.001; ****P< 0.0001). Details about statistical analyses are described in the figure legends. Data were visualized with GraphPad Prism V9.